Thesis for the Degree of Doctor of Philosophy

Study on Fabrication and Applications of Ultrasound Transducers Using Carbon Nano Materials with Optoacoustic Effect

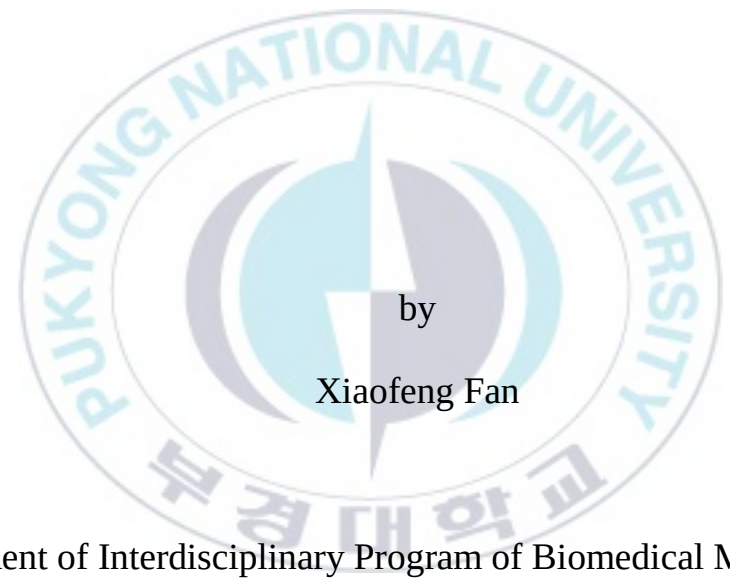

by

Xiaofeng Fan

Department of Interdisciplinary Program of Biomedical Mechanical

& Electrical Engineering

The Graduate School

Pukyong National University

August 2018

Study on Fabrication and Applications of Ultrasound Transducers Using Carbon Nano Materials with Optoacoustic Effect

광음향효과를 갖는 탄소나노재료를 이용한 초음파 트랜스듀서 제작 및 응용 연구

Advisor: Prof. Junghwan Oh

by

Xiaofeng Fan

A thesis submitted in partial fulfillment of the requirements for the degree of Doctor of Philosophy

Interdisciplinary Program of Biomedical Mechanical & Electrical Engineering

The Graduate School

Pukyong National University

August 2018

Study on Fabrication and Applications of Ultrasound Transducers Using Carbon Nano Materials with Optoacoustic Effect

A dissertation

by

Xiaofeng Fan

Approved by:

(Chairman) Prof. Kanglyeol Ha

(Member) Prof. Moojoon Kim

(Member) Prof. Jungsoon Kim

(Member) Prof. Hyun Wook Kang

(Member) Prof. Junghwan Oh

August 2018

Contents

List of Tables

List of Figures

Study on Fabrication and Applications of Ultrasound Transducers Using Carbon Nano Materials with Optoacoustic Effect

Xiaofeng Fan

Department of
Interdisciplinary Program of Biomedical Mechanical & Electrical Engineering
The Graduate School,
Pukyong National University

Abstract

The optoacoustic effect is the formation of sound waves following light absorption in a material sample. In order to obtain this effect the light intensity must vary, either periodically (modulated light) or as a single flash (pulsed light). The optoacoustic effect is quantified by measuring the formed sound (pressure changes) with appropriate detectors, such as microphones or piezoelectric sensors. The time variation of the electric output (current or voltage) from these detectors is the optoacoustic signal.

In the generation of ultrasound, pulsed laser beams are irradiated on a material and absorbed by it. The absorbed optical power is converted to heat, leading to rapid localized temperature increase. This results in rapid thermal expansion of a local region,

leading to generation of ultrasound into the medium. However, to obtain the ultrasound with high acoustic pressure, the materials to fabricate ultrasound transducers should have high efficiency of optical energy absorption and high thermal conductivity.

In this dissertation, the composite of carbon nanotubes (CNTs) and poly-dimethylsiloxane (PDMS) were coated on a polymethyl methacrylate (PMMA) plate to make optoacoustic transducers. Because of the high efficiency of optical energy absorption and high thermal conductivity, they can transfer the absorbed heat energy to a surrounding medium very rapidly and effectively.

The generated ultrasound waves by the optoacoustic transducer when irradiated a pulsed laser beam were measured using a needle hydrophone. It was shown that the generated ultrasound waves had the typical waveform of the blast wave. Some propagation characteristics of the blast wave were measured and compared with the calculated results. It was found that the propagation speed and attenuation of the wave are different from those of usual sound. And, from the comparison of the measured and the calculated acoustic fields, it is assumed that every point on the transducer surface produces almost same waveform.

In order to get much higher acoustic pressure by focusing, an optoacoustic film transducer was fabricated by coating carbon nanotubes (CNTs) and poly(dimethylsiloxane) (PDMS) on a surface of a flexible optical polyethylene terephthalate (PET) sheet with thin thickness. A line-focused optoacoustic source was made using the film transducer, and its characteristics were investigated. Very high pressure about 35 MPa in maximum was obtained by the source. It was demonstrated

that the source can engrave a line trace on a chalk surface.

The results suggested that the composite of light-absorbing material (CNTs) and elastomeric material (PDMS) can be used to fabricate an optoacoustic transducer and generate blast wave-like shock waves efficiently when the transducer is irradiated by a pulsed laser beam. The line-focused optoacoustic source fabricated by using the film transducer gives very high peak pressure at its focal position. From the line trace engraved on a chalk by the effect, it is suggested that the acoustic pressure for micro-scale ultrasonic fragmentation and biomedical therapy could be obtained by the line-focused optoacoustic source.

Ch. 1. Introduction

1.1. Backgrounds

The optoacoustic or photoacoustic effect is the production of acoustic waves by the absorption of light in a material sample [1, 2]. The optoacoustic effect was first discovered by Alexander Graham Bell in 1880 when he worked on a long-distance sound transmission without any cables [3]. He observed that sound waves were produced directly from a solid sample when exposed to beams of sunlight that were rapidly interrupted with a rotating slotted wheel [4].

The optoacoustic effect is based on the sensitive detection of acoustic waves launched by the absorption of pulsed or modulated laser radiation by means of transient localized heating and expansion in a material sample. When the sample is illuminated by the laser, some of the laser energy is absorbed by the molecules in the sample, thus resulting in a higher temperature of some region. The rise in temperature will generate an expanding region and a pressure wave will propagate away from the heat source [5, 6]. The pressure wave can be detected by using a piezoelectric or optical transducer.

Carbon nanomaterials have a very large surface area per unit mass and have unique optical properties. They have outstanding strength, and can be highly electrically conducting or semiconducting, may be as thermally conductive at room temperature as any other known material [7]. This range of unique properties of carbon materials have opened the doors to advances in performance in a wide range of materials and devices. Carbon nanomaterials have been attracting a great deal of research interest in the last

few years. Their unique electrical, optical and mechanical properties make them very interesting for developing the new generation of miniaturized, low-power, ubiquitous sensors or transducers.

Among the carbon nanomaterials, carbon nanotubes (CNTs) have become the subject of intense investigation since their discovery. Such considerable interest reflects the unique behavior of CNTs, including their remarkable electrical, chemical, mechanical, structural properties and strong light absorption characteristics [8, 9]. CNTs can display metallic, semiconducting and superconducting electron transport, possess a hollow core suitable for storing guest molecules and have the largest elastic modulus of any known material. The remarkable sensitivity of CNTs conductivity to the surface adsorbates permits the use of CNTs as highly sensitive nanoscale sensors. These properties make CNT extremely attractive for a wide range of electrochemical biosensors ranging from amperometric enzyme electrodes to DNA hybridization biosensors.

On the other hand, Extracorporeal Shock Wave Therapy (ESWT) is an 18-minute non-surgical procedure used to cure chronic plantar fasciitis, Achilles tendonitis, tennis elbow, shoulder tendonitis, and other chronic tendinopathies. Extracorporeal Shock Wave Lithotripsy (ESWL), a similar shock wave therapy procedure, is used regularly for breaking up and dispersing kidney stones. For ESWT or ESWL, very strong shock waves are usually needed.

A shock wave is an intense, but very short pulse wave traveling faster than the speed of sound [10]. Shock waves are formed when a pressure front moves at supersonic

speeds and pushes on the surrounding air [11]. A commonly known shock wave is the thunder following lightning. Shock waves are also associated with earthquakes, volcanic eruptions and explosion. Typical characteristics of shock waves:

- A short rise time on the order of a few nanoseconds reaching a peak pressure;
- After the rapid increase of pressure there is a longer period of decreasing pressure;
- Pressure returns to normal and then becomes negative;
- Negative pressure may cause cavitation effects.

However, it is not easy to produce artificial shock waves which have stable and repetitive waveforms. So far, it is known that those shock waves are generated in the focal zone of the concave transducers with electronic or electromagnetic effect. Recent studies show that a laser generated ultrasound optoacoustic transducer made by coating a composite of carbon nanomaterials and elastomers on a substrate can also generated shock waves because of the optoacoustic effect.

In H.W. Baac's study, a nanocomposite film of carbon nanotubes (CNTs) and elastomeric polymer is formed on concave lenses, and used as an efficient optoacoustic source [12]. The CNT-coated lenses can generate unprecedented optoacoustic pressures of 50 MPa in peak positive on a tight focal spot of 75 mm in lateral and 400 mm in axial widths. They observed strong shock waves at the lens focus upon excitation by pulsed laser irradiation. In R. J. Colchester's research, an optical ultrasound transducers were created by coating optical fibers with a composite of carbon nanotubes (CNTs) and polydimethylsiloxane (PDMS) using dip coating method [13]. Under pulsed laser excitation, ultrasound pressures of 3.6 MPa and 4.5 MPa at the coated end faces were

achieved with optical fiber core diameters of 105 and 200 μm, respectively. In B.Y. Hsieh's study, they demonstrated laser generated high intensity acoustic waves using carbon nanofibers–polydimethylsiloxane (CNFs-PDMS) thin films, and the maximum acoustic pressure they obtained is 12.15 MPa using a 4.2 mJ, 532 nm Nd:YAG pulsed laser [14].

However, the fabrication method of the optoacoustic transducer and fundamental characteristics of the shock waves have not been investigated in detail. Also, the higher acoustic pressure of the generated shock waves is needed for some biomedical applications, such as for ESWL or ESWT. Many more researches are needed to better understand the acoustic shock waves generated by the ultrasound optoacoustic transducers made of the composite of carbon nanomaterials and polymers with the optoacoustic effects when irradiated pulsed laser energy.

1.2. Purposes and outline

The purposes of this study are:

- To establish the fabrication method of optoacoustic transducers made of CNT/PDMS composite on a PMMA substrate.
- To investigate characteristics of the ultrasound shock waves generated by the optoacoustic transducers.
- To study on the feasibility of biomedical applications, such as for ESWT or ESWL, of the ultrasound shock waves.

The study will be described as following:

In Chapter 2, the mechanism of optoacoustic effect and the generated ultrasound waves by the optoacoustic effect are introduced. Then, basic knowledge related to shock waves, such as characteristics and applications, is introduced. At last, the basic theory of shock wave generation by ultrasound transducers with optoacoustic effect is introduced.

In Chapter 3, the characteristics of carbon nanomaterials, mainly the carbon nanotubes, are introduced. Then, the fabrication methods and process of optoacoustic transducers made of CNT/PDMS are introduced in detail. Two kind of optoacoustic transducers with different substrates were fabricated.

In Chapter 4, the characteristics of generated ultrasound waves by the fabricated two kind of CNT/PDMS optoacoustic transducers are measured separately. The relation between the generated acoustic pressure and thickness of CNT/PDMS film is discussed.

The propagation characteristics are also measured.

In Chapter 5, the waveform of the generated ultrasound by the CNT/PDMS optoacoustic transducers is confirmed using NDT transducers. The wave is simulated using PiezoCAD and the results are compared with that measured using commercial PVDF and fiber optic hydrophones.

In Chapter 6, the applications of the CNT/PDMS optoacoustic transducer are introduced. A line-focused source was fabricated using the flexible CNT/PDMS optoacoustic transducer. The characteristics and applications are introduced in detail.

In Chapter 7, conclusions are given and future work are listed.

Ch. 2. Theory of shock wave generation by ultrasound transducers with optoacoustic effect

2.1. Shock waves

Strong shock waves, like blast waves, move faster than the local speed of sound in a medium [15]. Like an ordinary wave, a shock wave carries energy and can propagate through a medium. However, it is characterized by an abrupt, nearly discontinuous change in pressure, temperature and density of the medium. Naturally, a shock wave can be produced in an explosion because of the rapid energy release which generates a pressure wave of finite amplitude. During the volcano eruption and flying of airplane, shock waves are also formed when a pressure front moves at supersonic speeds and pushes on the surrounding air.

2.1.1. Physics of shock waves

Physical variables describing shock wave

The International Electrical Conference devised a draft set of definitions to become the standard for shock wave measurements. According to these standards the Technical Working Group of the German Society of Shock Wave Lithotripsy has generated a selection of useful variables to define a focused shock wave source [16].

Peak positive pressure, P+: During the time course of a single shock wave the pressure increases sharply at the beginning to reach its maximum, the pressure P+ (Fig. 2-1). This value varies with the energy setting of the device and should be reported at

the lowest, medium and highest energy level available. The maximum pressure point is called the focus, and is surrounded by a focal zone.

6 dB zone: This is the zone around the focus, where half of the original P+ is measured. The volume of this zone is defined by its extent along the x, y, and z axes.

5 MPa focal extent: In contrast to the above variables the 5 MPa zone is defined by the absolute values of the 5 MPa isobar, which was chosen arbitrarily and represents a low pressure zone, which may or may not be a threshold for the medical effects of shock waves on living tissue.

Shock wave energy: The shock wave energy is defined as the time integral over the pressure time function of a given shock wave. The shock wave energy is required to be declared in a well-defined area such as the focal areas mentioned above.

Energy flux density: This is defined as a certain amount of energy passing through a defined area (mJ/mm^2). This variable is used to describe the power of a given lithotripter or treatment arrangement, e.g. low-energy vs high-energy treatment strategies in orthopaedic shock wave therapy.

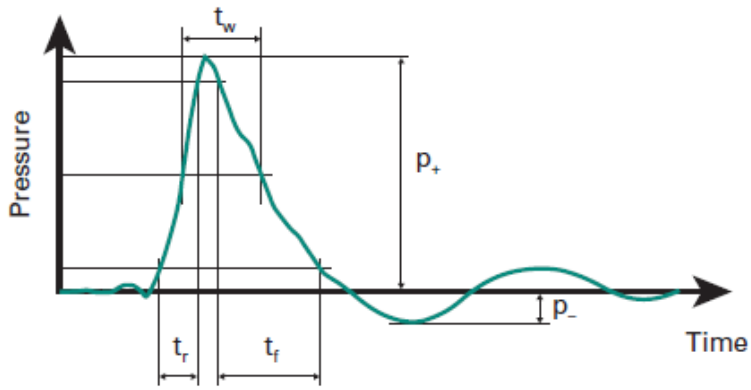

Fig. 2-1 The pressure-time relationship of a typical shock wave with a sharp initial positive rise and subsequent negative pressure [17].

Cavitation in shock waves

In addition to direct shock wave effects, cavitation generated by the negative pressure phase of shock waves occurs in the fluid surrounding stones and within micro cracks or cleavage interfaces. For initial fragmentation, cavitation is less relevant but becomes important as stone fragments become smaller. Cavitation-induced erosion is especially observed at the anterior surface of stones [18]. Suppression of cavitation using highly viscous media, hyper pressure, or overpressure significantly reduces disintegrative shock wave efficacy [19]. Recognition of the role of cavitation in stone comminution has led to efforts to enhance the action of cavitation bubbles, such as tandem shock waves generated using a piezoelectric source fitted to an electrohydraulic system, with an additional discharge circuit to produce the second pulse [20]. However, cavitation can be detrimental to fragmentation, as it results in production of gas bubbles lasting for many seconds, therefore attenuating subsequent impulses [21].

Generation of shock waves

Four generating principles are used in clinical lithotripters. In electrohydraulic lithotripters (EHLs), a spark discharge between two electrodes produces the shock wave. EHLs have a great shot-to-shot variability, as the spark location varies as the electrodes wear down. The significance of this "jitter effect" is under debate [22], with some suggesting that it might be less relevant in large-focus sources [18]. The electro conductive system employs electrodes surrounded by a highly conductive solution, resulting in repeatable spark location because of shorter inter electrode distance and reduced electrode wear [23]. Electrode life time exceeds 40,000 impulses. Electromagnetic and piezoelectric sources provide stable shock wave release lasting for more than a million shocks; however, acoustic output instability may occur [24].

Measurement of shock wave pressures

Beyond the technique of optical visualization of sound waves with high-speed cameras in two dimensions (Schlieren optical measurement), which is too slow, the most widely used instruments to measure shock-wave pressure are the so-called hydrophones. Essentially these are microphones that are used underwater to receive the sound waves of a given shock-wave source. To measure a pressure-field distribution, the hydrophone has to be moved around and repetitive measurements made. In particular the PVDF hydrophones are very sensitive and become worn during repeated measurements [25], but fiber-optic hydrophones are being used to measure shock wave pressures. They measure the varying density of water during the time of passage of a shock wave front [26]. As a surrogate, some researchers use human or artificial stones which are subjected to fragmentation by multiple shock waves in an in vitro system until they are completely disintegrated. The number of shock waves necessary for complete disintegration is then

counted [27].

2.1.2. Application of shock waves

A lithotripter is constructed using various components, i.e. the shock wave source, the shock wave focusing element, the coupling device for shock waves and the calculus imaging unit [28]. All components are important in ensuring that stones are disintegrated successfully.

There exist three fundamental types of clinical extracorporeal shock wave lithotripters: electrohydraulic, electromagnetic, and piezoceramic [29] (see Fig. 2-2). In electrohydraulic lithotripters, an underwater spark generates a shock wave that is focused on the kidney stone by an ellipsoidal reflector. The first and most common lithotripter, the Dornier HM3, is considered the gold standard because of its high long-term stone free rates (67–90%) for a wide range of stones. New electrohydraulic lithotripters incorporate longer lasting electrodes, which provide repeatable waveforms. Electromagnetic lithotripters conduct high current through a coil, which then repulses a parallel plate. Lenses or reflectors focus the wave created by the displacement of the plate. Piezoceramic lithotripters are generally arrays built on a spherical segment. Array technology allows steering of the beam and even image tracking of the stone. Sufficiently powerful compact devices are being developed with stacked composite elements [30] or electrically prestressed piezoelectric material [31].

Lithotripters are commonly compared on the basis of the product of the peak pressure at the focus and the -6dB pressure volume, which ranges from 0.2 to 10 cm^3. Since peak pressures are so varied, it might be more logical to compare the volume in

which a super threshold pressure is produced. However, this threshold value has not been determined yet, and a higher product correlates with improved clinical efficacy. Electrohydraulic lithotripters, particularly the HM3, produce low peak pressures (30–40 MPa) but the largest focal volume and the largest product. Newer electromagnetic and piezoceramic lithotripters generally produce more tightly focused beams and higher peak pressures, with the notable exception of the low-amplitude, broad focused lithotripter developed by Eisenmenger [32]. A fourth type of extracorporeal lithotripter uses a laser source and optoacoustic transduction to generate shock waves (see Fig. 2-2). A prototype of the laser lithotripter has been built but is not yet used clinically [33]. Sparks, mechanical drills, and lasers are also used intra corporeally to break stones.

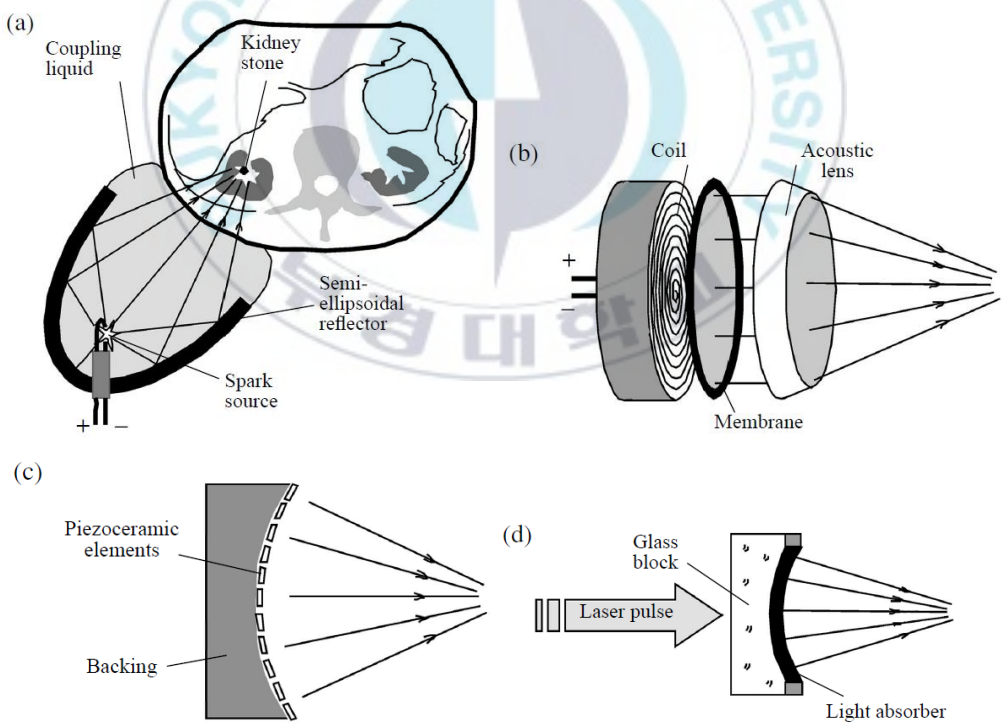

Fig. 2-2 Three clinical and one research lithotripter designs. Electrohydraulic machines

(a) use an ellipsoidal reflector to focus the shock wave generated by an underwater spark. Electromagnetic devices (b) employ impulsive displacement of a plate to generate the wave, which is focused by a lens or reflector. Piezoceramic lithotripters (c) utilize the waves generated by piezoelectric elements. The laser lithotripter (d) relies on the conversion of an optical wave to an acoustic one in a thin spherical layer of a light-absorbing liquid [29].

2.2. Ultrasound with optoacoustic effect

2.2.1. Optoacoustic effect

Optoacoustic effect or photoacoustic effect is the production of acoustic waves by the absorption of light in a material. The optoacoustic effect is based on the sensitive detection of acoustic waves launched by the absorption of pulsed or modulated laser radiation by means of transient localized heating and expansion in a material sample. When the sample is illuminated by the laser, some of the laser energy is absorbed by the molecules in the sample, thus resulting in a higher temperature of some region. The rise in temperature will generate an expanding region and a pressure wave will propagate away from the heat source. The pressure wave is periodic and can be detected by using a pressure transducer.

During an optoacoustic measurement the sample is enclosed in a small, tightly closed sample compartment called optoacoustic cell which is cylindrical in shape. The optoacoustic effect is based on the sensitive detection of acoustic waves launched by the absorption of pulsed or modulated laser radiation via transient localized heating and expansion in a gas, liquid, or solid. When the laser hits the sample, some of the energy

is absorbed by the molecules in the samples resulting in a region of higher temperature. The rise in temperature will generate an expanding region and a pressure wave will propagate away from the heat source. The periodic pressure wave can be detected using a pressure transducer in contact with the sample. The signal of the pressure transducer is proportional to the amplitude of the pressure wave. Fig.2-3 shows the block diagram of the evaluation of optoacoustic signal generated from optoacoustic effect.

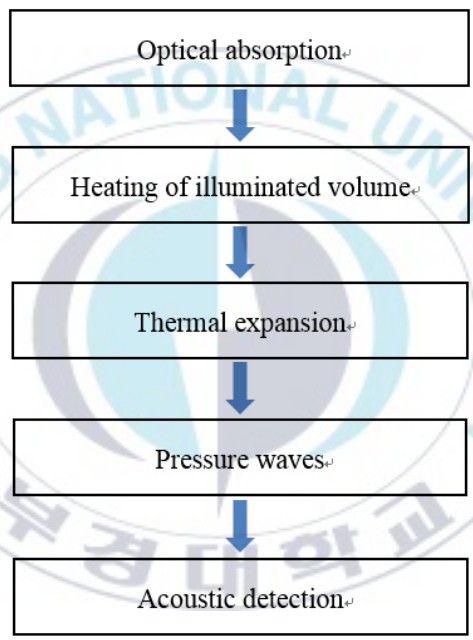

Fig. 2-3 Block diagram for evaluation of optoacoustic signal.

An optoacoustic spectra of the sample can be taken by continuously tuning the wavelength of the exciting light source and taking the optoacoustic signal at each wavelength. If the optical wavelength couples to an energy transition in the sample material, there will be a variation in the optoacoustic signal. The optoacoustic spectra give many valuable information regarding the sample.

2.2.2. Laser generated ultrasound

Laser generation of ultrasound was first demonstrated by White [34]. Since then, lasers have been used to generate ultrasound in solids, liquids, and gases for a number of applications. A comprehensive review of laser generation of ultrasound is given in Hutchins [35], and Scruby and Drain [36]. Here, the generation of ultrasound in solids using pulsed lasers will be discussed in detail.

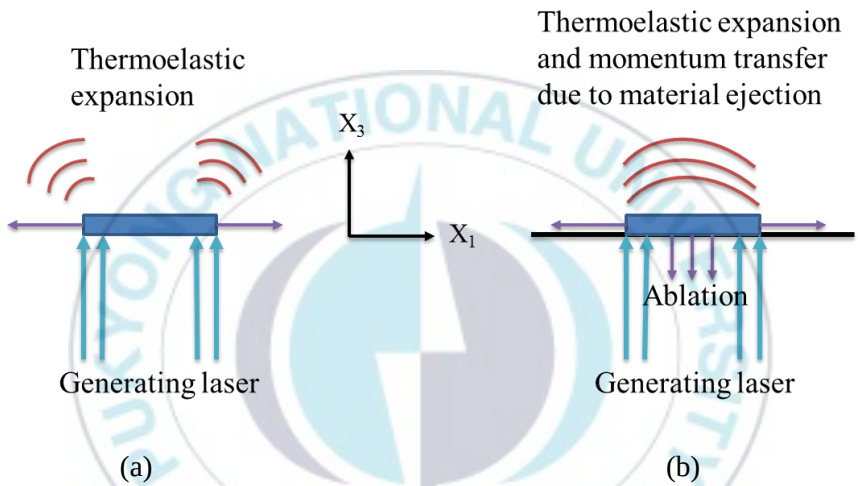

Fig. 2-4 Laser generation of ultrasound in (a) thermoelastic regime and (b) ablative regime. [37]

It is easy to outline the dominant mechanisms involved in the laser generation of ultrasound in a solid. A pulsed laser beam impinges on a material and is partially absorbed by it. The optical power that is absorbed by the material is converted to heat, leading to rapid localized temperature increase. This results in rapid thermal expansion of a local region, which leads to generation of ultrasound into the medium. If the optical power is kept sufficiently low enough that the material does not melt and ablate, the generation regime is called thermoelastic (see Fig. 2-4(a)) [37]. If the optical power is

high enough to lead to melting of the material and plasma formation, once again ultrasound is generated, but in this case via momentum transfer due to material ejection (see Fig.2-4(b)). The ablative regime of generation is typically not acceptable for nondestructive characterization of materials. However, it is useful in some process monitoring applications, especially since it produces strong bulk wave generation normal to the surface. In some cases where a strong ultrasonic signal is needed but ablation is unacceptable, a sacrificial layer (typically a coating or a fluid) is used either unconstrained on the surface of the test medium or constrained between the medium and an optically transparent plate. The sacrificial layer is then ablated by the laser, again leading to strong ultrasound generation in the medium due to momentum transfer.

2.3. Theory of the ultrasound generation with optoacoustic effect

The most common mechanism of optical generation of ultrasound is the thermoelastic effect [34, 38, 39]. A laser pulse is focused onto a light-absorbing film deposited on a transparent substrate. Optical absorption rapidly heats a localized volume, in which thermal expansion launches an acoustic wave into the overlying sample. The major drawback of the thermoelastic effect always has been poor conversion efficiency [40, 41]. In this section, the waveform generated by the optoacoustic effect in a CNT/PDMS material is driven theoretically, and the conversion efficiency is estimated.

Acoustic wave generation with thermoelastic effect is governed by two equations: the heat conduction equation and the acoustic wave equation. The heat conduction equation, which determines the temperature distribution, is shown in the following expression [39]:

$$\frac{\partial T}{\partial t} = k\nabla^2 T + \frac{1}{\rho C_p} h(\vec{r}, t) \quad , \tag{2-1}$$

where, k is the thermal diffusivity, T is the increased temperature above the ambient temperature, ρ is the density, C_p is the specific heat capacity, and h is the rate of energy deposited per unit volume in the medium of the CNT/PDMS composite material. In this case, energy is deposited by optical absorption of a pulsed laser.

The wave equation with the heat source which generates ultrasound by the optoacoustic effect is given by [38, 42]:

$$\nabla^2 \emptyset - \frac{1}{c^2}\frac{\partial^2 \emptyset}{\partial t^2} = \frac{3B}{\rho c^2}\alpha_L T \ , \tag{2-2}$$

where, $\emptyset$ is the scalar potential, c is the longitudinal wave speed, B is the bulk modulus, α_L is the linear coefficient of thermal expansion in the medium.

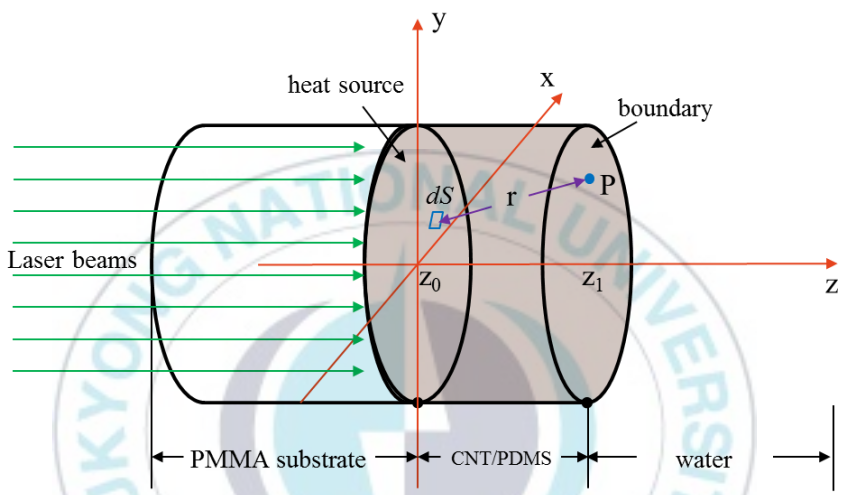

Fig. 2-5 Coordinate system for sound generation analysis in the CNT/PDMS optoacoustic transducer.

As shown in Fig. 2-5, it is assumed that the surface of heat source is on z_0, and the boundary between the CNT/PDMS and water is on z_1. The potential on z_1 is obtained by the Eq. (2-3).

$$\emptyset = -\frac{1}{4\pi}\frac{3B\alpha_L}{\rho c^2}\int_S \frac{T\left(t-\frac{r}{c}\right)}{r} dS, \tag{2-3}$$

where, r is the distance from a point on the surface of heat source to a point on the boundary. It is known that the surface of the CNT/PDMS film irradiated by a laser beam

is divided into small elements with dS. It is assumed that there is no attenuation in the medium.

The relationship between sound pressure p and $\emptyset$ is:

$$p = -\rho \frac{\partial \emptyset}{\partial \mathrm{t}} \tag{2-4}$$

Substituting Eq. (2-3) into Eq. (2-4), then,

$$p = \frac{1}{4\pi} \frac{3B\alpha_L}{c^2} \frac{\partial}{\partial \mathrm{t}} \int_S \frac{T(t-\frac{r}{c})}{r} dS \tag{2-5}$$

By dividing the laser irradiated area into small elements with $\Delta S = \Delta x \Delta y$, and dividing them into L and M sections in the x-axis and y-axis directions, respectively, Eq. (2-5) can be changed to:

$$p = \frac{1}{4\pi} \frac{3B\alpha_L}{c^2} \Delta x \Delta y \sum_{l=1}^{L} \sum_{m=1}^{M} \frac{\frac{\partial}{\partial \mathrm{t}} T(t-\frac{r}{c})}{r} \tag{2-6}$$

Assuming that the pulse width of the laser irradiated on the z_0 plane is sufficiently short and the thermal diffusivity is ignored during the generation of the ultrasonic wave. Then, from Eq. (2-1)

$$\frac{dT(t)}{dt} = \frac{1}{\rho C_p} h(t) \tag{2-7}$$

Substituting (2-7) into (2-6) yields:

$$p = \frac{1}{4\pi}\frac{3B\alpha_L}{\rho c^2 C_p}\Delta x \Delta y \sum_{l=1}^{L}\sum_{m=1}^{M}\frac{h(t-\frac{r}{c})}{r} \quad (2\text{-}8)$$

If the rate of energy deposited per unit volume $h(t)$ or the temperature profile $T(t)$ on the source plane is known, the pressure at point P on the CNT/PDS and water boundary is obtained.

On the other hand, the ratio of the thermal energy absorbed from the laser and stored in the absorber is estimated by the following equation:

$$\eta = \frac{T_H}{T_L} \times \left\{1 - \exp(-\frac{T_L}{T_H})\right\}, \quad (2\text{-}9)$$

where, T_L is the duration of the laser pulse, T_H is the thermal diffusion time.

$$T_H = \frac{d^2}{16k_x}, \quad (2\text{-}10)$$

where, d is the diameter of the internal structure, k_x is the thermal diffusivity of the surrounding material.

In the CNT/PDMS transducer, d is about 25 nm of CNT diameter, the thermal diffusivity of PDMS is $k_x = 1.06 \times 10^{-7}$ $[m^2/s]$. Pulse width of the laser is $T_L = 6\sim9\ ns$. Then $\eta = 0.04\sim0.06$. Laser energy remaining in CNT after laser irradiation is very small about 5%. That is, most of the laser energy is transferred to the PDMS. The

PDMS has very high thermal expansion coefficient of $\alpha_L = 0.92 \times 10^{-3}\ [K^{-1}]$, so that the mechanical to acoustic energy conversion ratio is higher than other materials. Even the energy conversion ratio is less than 5%, the high pressure ultrasonic waves can be generated if a high power laser is used.

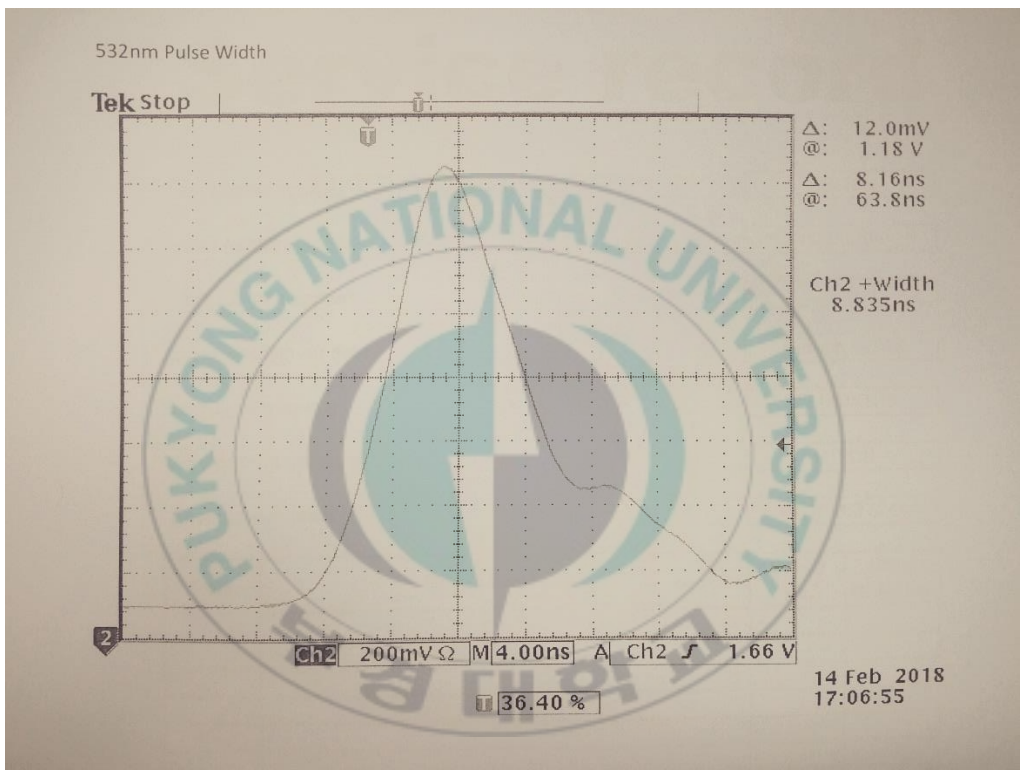

Fig. 2-6 Pulse width of the 532 nm-wavelength pulsed laser used in the experiment.

2.4. Simulation

The sound pressure waveform at a certain point on the boundary between the CNT/PDMS and water can be obtained by equation (2-6). To use Equation (2-6), the temperature profile on the source plane $T(t,\ 0)$ by a laser irradiation should be known.

However, the value is difficult to grasp accurately. Therefore, the shapes of the sound pressure waveforms were predicted by assuming the temperature profiles as following:

- **Assumption 1:** The radius of the CNT/PDMS film is at an arbitrary point in infinite water (that point is $z = 0$, xy plane), a short pulse laser is irradiated to the film, and the intensity is constant.
- **Assumption 2:** As shown in Fig. 2-6, according to the pulse width of the 532 nm-wavelength pulsed laser used in the experiment, the temperature on the surface of the heat source increases during the laser pulse duration (8 ns), and then decreases after the laser pulse duration.

$$T(t) = A\,(t - r/c)\exp(-t/T_L) \tag{2-11}$$

where, $A = 1 \times 10^7$ is a constant, T_L is the duration of the laser pulse, r is the distance from a point on the surface of heat source to a point on the boundary between the surface of the CNT/PDMS optoacoustic transducer and water, and c is the wave speed in the medium.

Figure 2-7(a) and 2-7(b) show the simulation results of temperature profiles and sound pressure waveform, respectively, when the distance from a point on the surface of heat source to a point on the boundary are $r = 8\ \mu m, 10\ \mu m, 12\ \mu m,$ and $14\ \mu m$. From these results, it can be seen that the temperature profiles on the surface of heat source increase during the laser pulse duration quickly and decrease after the laser pulse duration. The sound pressure waveform has a very short impulse shape, the pulse width of -6 dB is about 4 ns. With the increase of distance r, the magnitudes of temperature

profiles and sound pressure waveforms decrease respectively, while they keep the same shape.

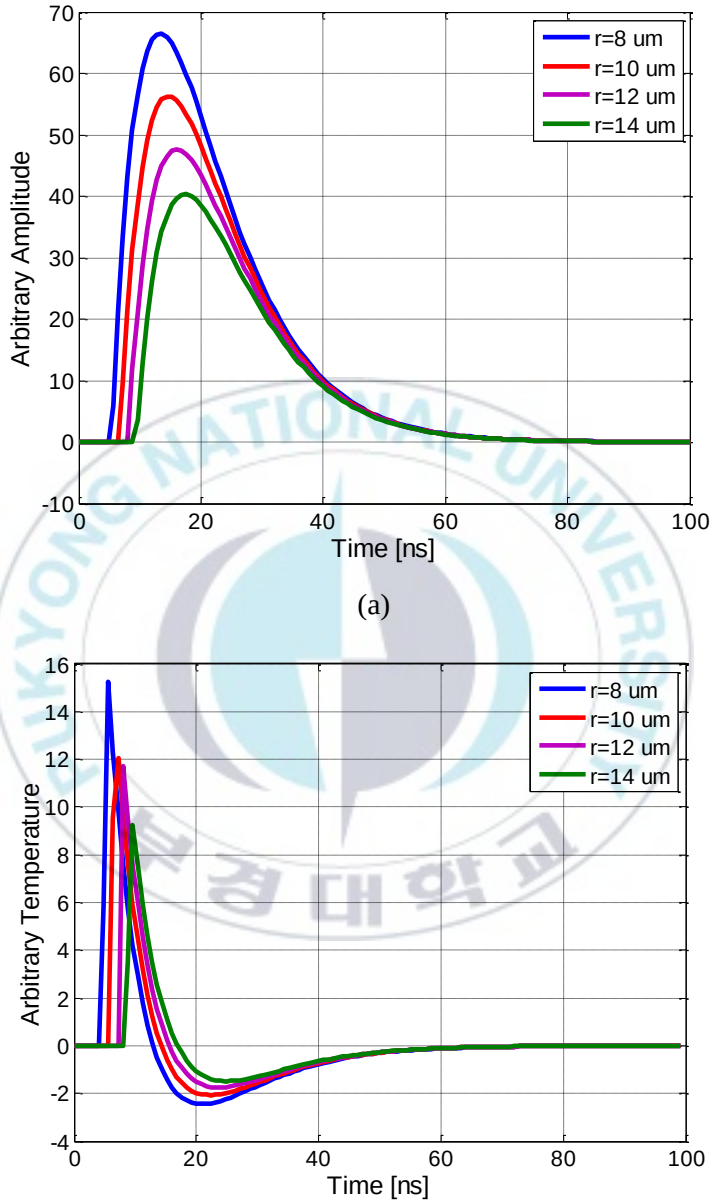

Fig. 2-7 Simulation results of the variation of temperature profiles (a) and sound pressure waveform (b) with distance r.

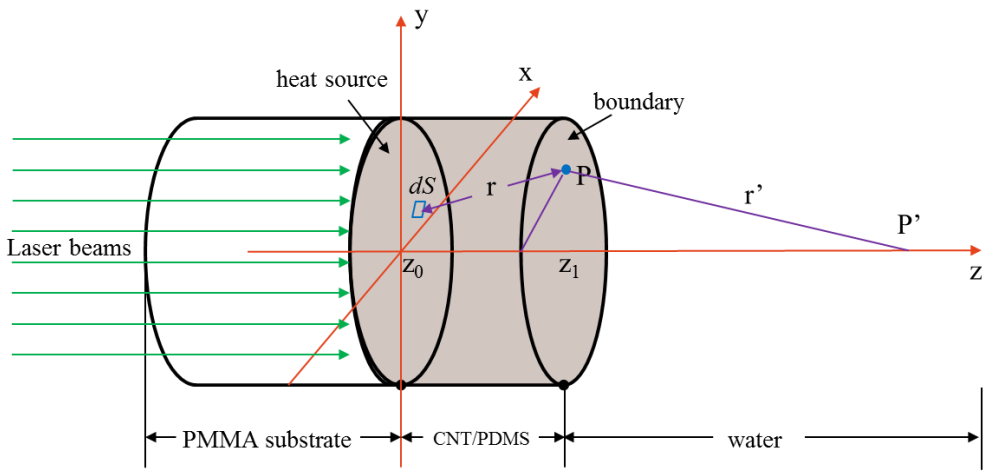

Fig. 2-8 Coordinate system for the generated sound wave propagation in water.

As shown in Fig. 2-8, the sound pressure $P(t)$ at point P′ in water is simulated from the sound pressure at every point P in the boundary.

$$P(t) = A\left(1 - \frac{t-T_H}{T_L}\right)\exp\left(-\frac{t}{T_L}\right)\exp(-\alpha r'), \quad (2\text{-}12)$$

where, T_L is the duration of the laser pulse, T_H is the thermal diffusion time, $\alpha = 0.24\ dB/cm$ is the attenuation coefficient of sound pressure in water, and r' is the distance between the point P on the boundary and point P′ in water.

Figure 2-9 shows the sound pressure waveform at point P′ in water when the distance r′ = 1 cm. The waveform is similar to the sound pressure waveform at point P on the boundary. Fig. 2-10 shows the sound pressure distribution in water when $r' = 1\ cm \sim 6\ cm$. The sound pressure waves have the same waveform while the magnitudes decrease when the distance r' increases.

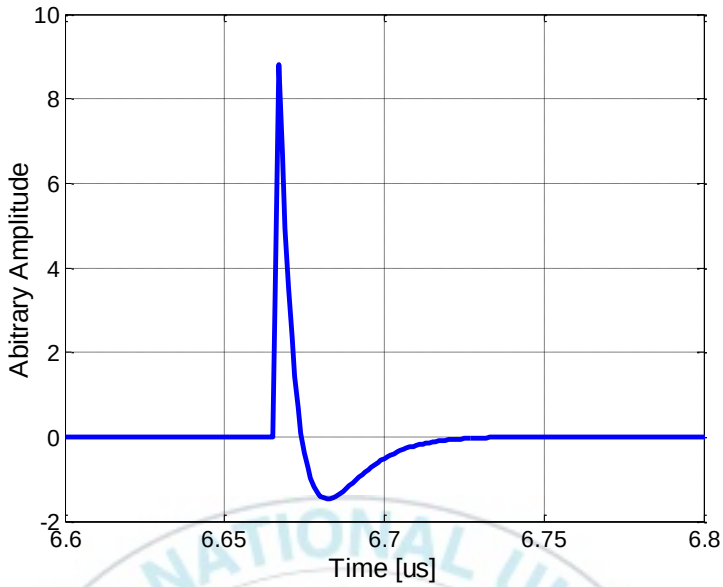

Fig. 2-9 Simulation results of the sound pressure at point P′ in water when $r' = 1\ cm$.

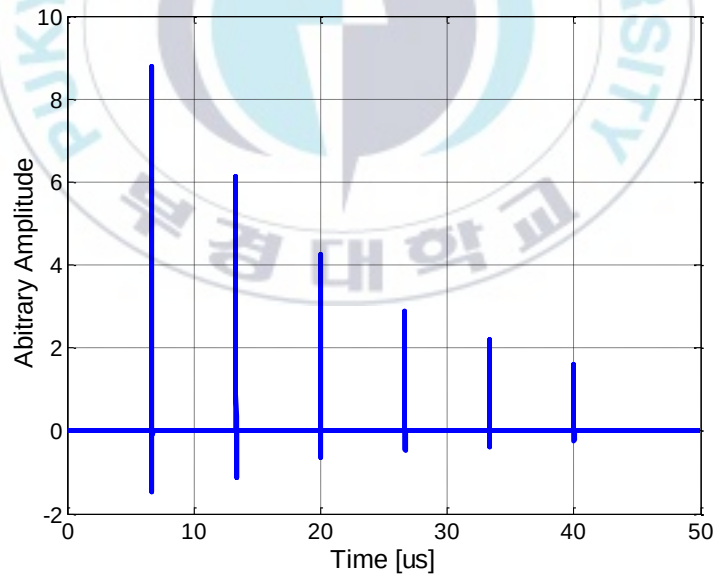

Fig. 2-10 Simulation results of the sound pressure distribution in water when $r' = 1\ cm \sim 6\ cm$.

2.5. Summary

Optoacoustic effect is the production of acoustic waves by the absorption of light in a material. When the laser irradiates on a sample, some of the energy is absorbed by the molecules in the samples resulting in a region of higher temperature. The rise in temperature will generate an expanding region and a pressure wave will propagate away from the heat source. With the heat conduction equation and the acoustic wave equation, the ultrasound waves generated by optoacoustic effect can be simulated.

Ch. 3. Fabrication of optoacoustic transducers using carbon nanomaterials

In this chapter, the characteristics of carbon nanomaterials, especially carbon nanotubes (CNT), are discussed. Then, the fabrication methods of CNT films are introduced. At last, the fabrication process of CNT/PDMS optoacoustic transducers with two kinds of substrates (PMMA and PET) are described and summarized.

3.1. Carbon nanotube (CNT)

Carbon nanomaterials have outstanding strength, can be highly electrically conducting or semiconducting, may be as thermally conductive at room temperature as any other known material, have a very large surface area per unit mass, and have unique optical properties. This range of unique properties has opened the doors to advances in performance in a wide range of materials and devices. Carbon nanomaterials have been attracting a great deal of research interest in the last few years. Their unique electrical, optical and mechanical properties make them very interesting for developing the new generation of miniaturized, low-power, ubiquitous sensors or transducers.

Among the carbon nanomaterials, carbon nanotubes (CNTs) have become the subject of intense investigation since their discovery. Such considerable interest reflects the unique behavior of CNT, including their remarkable electrical, chemical, mechanical, structural properties and strong light absorption characteristics. CNT can display metallic, semiconducting and superconducting electron transport, possess a hollow core suitable for storing guest molecules and have the largest elastic modulus of any known

material. The remarkable sensitivity of CNT conductivity to the surface adsorbates permits the use of CNT as highly sensitive nanoscale sensors. These properties make CNT extremely attractive for a wide range of electrochemical biosensors ranging from ampere metric enzyme electrodes to DNA hybridization biosensors. Also, the CNTs have high optical absorption, efficient heat transduction, and high thermal expansion.

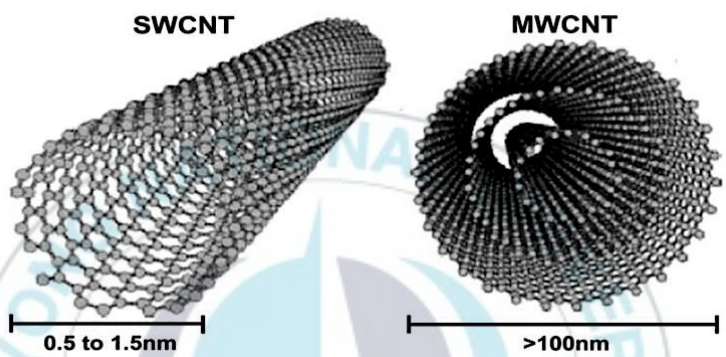

Fig. 3-1 Structure of the single-wall nanotubes (SWNTs) and multi-wall nanotubes (MWNTs).

Carbon nanotubes (CNTs) are members of the fullerene structural family and the ends of a nanotube may be capped. Their name is derived from their long, hollow structure with the walls formed by graphene sheets. These sheets are rolled at specific and discrete ("chiral") angles, and the combination of the rolling angle and radius determines whether the individual nanotube shell is metallic or semiconducting. CNTs are categorized as single-wall nanotubes (SWNTs) and multi-wall nanotubes (MWNTs). Fig. 3-1 shows the structure of the SWNTs and MWATs. Multi-wall nanotubes (MWNT) consist of multiple rolled layers (concentric tubes) of graphene. Individual CNTs naturally align themselves into "ropes" held together by van der Waals forces, more specifically, pi stacking. The chemical bonding of CNTs is composed entirely of sp2

bonds, similar to those of graphite. These bonds, which are stronger than the sp3 bonds found in alkanes and diamond, provide CNTs with their unique strength. Such strong bonds are characterized by a low chemical reactivity with the molecular environment. Consequently, the functionalization of the carbon nanotube sidewalls is mandatory to improve both the sensitivity and the selectivity of CNT based gas sensors [11].

3.2. Polydimethylsiloxane (PDMS)

Table 3-1 Physical properties of the materials used for fabrication of the CNT/PDMS optoacoustic transducers.

Materials	Density (Kg/m^3)	Specific heat capacity ($J/Kg \cdot K$)	Thermal conductivity ($W/m \cdot K$)	Speed of sound (m/s)
PMMA	1190	1420	0.19	2690
CNT film	440	460	0.46	2130
PDMS	970	1460	0.16	987
Water	998	4200	0.6	1481

Polydimethylsiloxane (PDMS) belongs to a group of polymeric organosilicon compounds that are commonly referred to as silicones. PDMS is the most widely used silicon-based organic polymer, and is particularly known for its unusual rheological (or flow) properties. PDMS is optically clear, and, in general, inert, non-toxic, and non-flammable. It is also called dimethicone and is one of several types of silicone oil (polymerized siloxane). Its applications range from contact lenses and medical devices to elastomers; it is also present in shampoos (as dimethicone makes hair shiny and

slippery), food (antifoaming agent), caulking, lubricants and heat-resistant tiles. Table 3-1 shows the properties of the materials.

3.3. Fabrication of the CNT/PDMS optoacoustic transducer

3.3.1. Methods of CNT coating

CNT based thin films have been prepared by various techniques. In this section, common techniques for coating CNTs films will be introduced.

(1) Dip-coating:

Dip-coating is a facile solution based surface coating method providing great potential to scale up for large scale coating and does not require sophisticated apparatus [43]. Essentially, the substrate is immersed into the CNTs based dispersion at a constant speed and remains inside for a period of time then starts to be pulled up. The pull up process needs a constant speed on carrying out to avoid any jitters. A thin layer of dispersion will be picked up with the substrate and a thin film forms after the drying process (Fig. 3-2(a)). The amount of captured dispersion depends on several factors: the dispersion viscosity, immersion time, pull-up speed (usually faster withdrawal gives thicker coating layer) and the interaction between the dispersion and substrate. The quality of the thin film is also affected by the drying process. One drawback of the dip-coating technique is that the fabrication process occurs at both sides of the substrate, which may restrict its application.

Introducing surfactants such as Triton X-100 and SDS would improve the dispersibility of CNTs for dip-coating. To improve the adhesion between substrate and film, pretreatment of substrate is necessary. Aminopropyltriethoxysilane is usually used for substrate treatment as an adhesion promoter by forming an interlayer between CNTs and substrate.

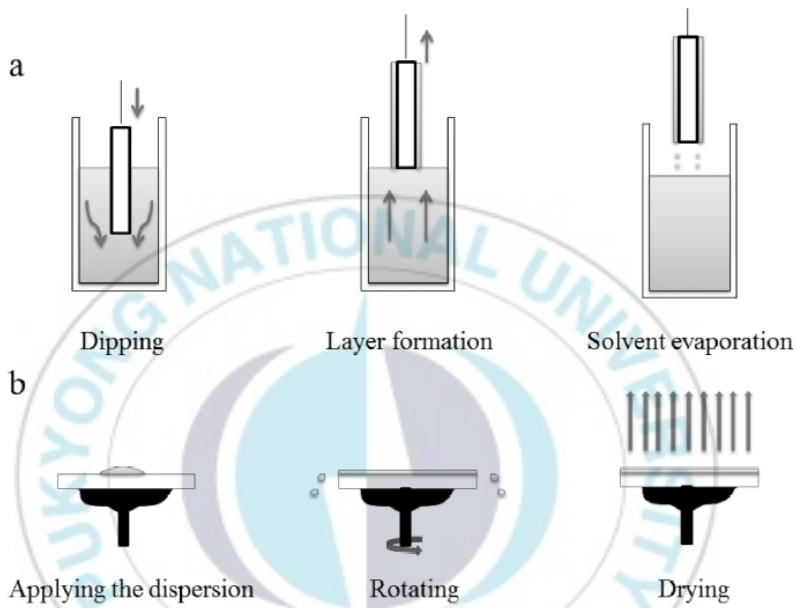

Fig. 3-2 Schematic diagrams of thin film preparation using dip-coating (a) and spin-coating (b) [43].

(2) Spin-coating:

Fabrication of CNTs based thin films using spin coating method involves depositing a mall puddle of CNTs based dispersion onto the center of a substrate, then spinning the substrate to high speed allowing dispersion to spread and cover the substrate to form a thin film by centrifugal force (Fig.3-2(b)) [43].

The thickness of film normally relates with the dispersion viscosity, angular speed and spin time. The orientation of CNTs appeared to have an angle of approximately 45℃ relative to the radial direction of the film, which is independent on the spin rare and radial position [44]. Themorphology of the thin film is also highly affected by the concentration of CNTs [45]. AFM study showed if SWCNTs concentration in blended solution is more than 2 wt. %, there is no interconnected phase separation microstructure and no island phase separation appeared on the film; the carbon nanotubes tend to aggregate. If the SWCNTs concentration equals to 1wt. %, the interpenetrating network phase separation microstructure can be formed. Nevertheless, when the concentration drops below 0.5 wt. %, result would only show island phase separation microstructure.

There exist a few drawbacks of spin-coating technique. Firstly, spin-coating is not suitable for large scale coating because large substrates cannot be spun at a sufficiently high rate to form a uniform layer. Secondly, the non-uniform distribution of materials along the radial direction becomes worst when scaling up the dimension. In addition, for multilayer film fabrication, the multiple spin coating process is too cumbersome. Last but not least, the spin-coating method lacks material efficiency. In a typical deposit process, most material is flung off and disposed.

(3) **Vacuum filtration:**

Vacuum filtration is a simple method to separate CNTs composites from solvents and compact into films which is achieved based on the different pressures between two sides Buchner funnel. The thin film formed is then peeled off from the filter paper and subjected to drying process. Despite the aforesaid advantages, the thin films made by vacuum filtration are usually quite thick, thus may not be preferred for certain

applications. Furthermore, film transfer is necessary as the peeled film could not be directly used for device applications.

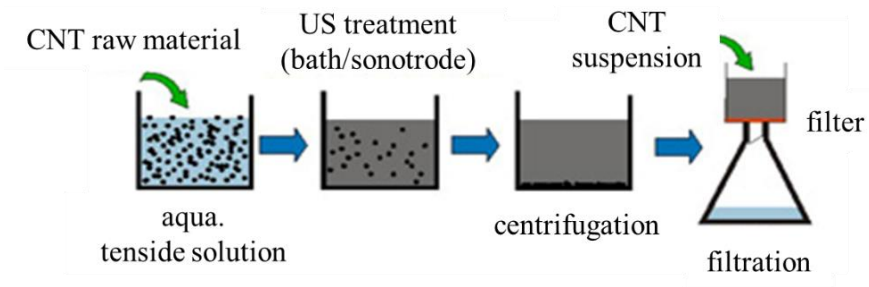

Fig. 3-3 Schematic diagrams of thin film preparation using vacuum filtration method.

In the fabrication process of CNT thin film using vacuum filtration method, the CNT raw materials first dissolved in the aqua tenside solution. Then, the mixed solution is bathed with ultrasound treatment using sonotrode to intensively make the particles dispersion well. The bathed solution is separated two parts after centrifugation, and the CNT suspension in the upper part is then pour in a beaker in the filtration system. The CNT film is fabricated after the solvent water is removed by the filtration system. Fig. 3-3 shows the process for vacuum filtration method.

In the vacuum filtration method, homogeneity of the films is guaranteed by the process itself. Because of their extreme rigidity (for objects of such small diameters), the nanotubes have long persistence lengths. The film thickness is readily controlled, with nanoscale precision, by the nanotube concentration and volume of the suspension filtered.

(4) Chemical vapor deposition (CVD):

Chemical vapor deposition (CVD) is a chemical process used to grow thin films. The substrate is exposed to one or more vaporized substances, and the vapor is thermally decomposed or reacted with other gases on the substrate surface to form thin film (Fig. 3-4). CVD is capable of producing CNTs thin films on various substrates. CNTs thin film can be grown on substrate by simultaneously providing organometallic and hydro carbon compounds in the method of CVD called spray pyrolysis. For the CVD process, catalysts are usually introduced in the growth process to promote the reaction. Ferrocene ($FeCp_2$) dissolved in benzene [46] and cyclohexane [47] are commonly used carbon resources. CVD method is used for one-step deposition or multiple depositions. Different types of CVD have been employed to form different CNTs based composite film.

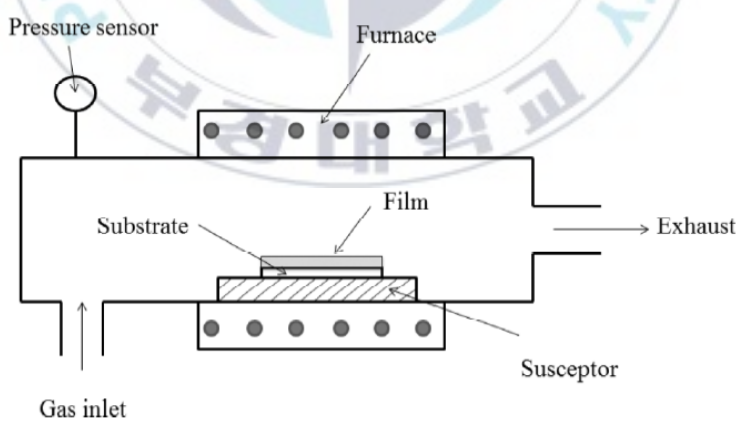

Fig. 3-4 Schematic diagram of typical thin film deposition using CVD method [43].

3.3.2. Fabrication process of the optoacoustic transducer

Two kind of CNT/PDMS optoacoustic transducers were fabricated using the vacuum filtration method. One was fabricated by coating the CNT/PDMS films on the surface of a poly(methyl methacrylate) (PMMA) substrate, and the other one was fabricated by coating the CNT/PDMS films on the surface of a thin flexible optical poly(ethylene terephthalate) (PET) sheet.

(1) Fabrication process of the optoacoustic transducer with PMMA substrate

Figure 3-5 shows the structure of the CNT/PDMS optoacoustic transducer. The CNTs and PDMS films were coated on a poly(methyl methacrylate) (PMMA) substrate. The diameter of the circular CNT/PDMS film is 40 mm. The size of the PMMA substrate is $50\ \text{mm} \times 50\ \text{mm}$ with the thickness of 10 mm.

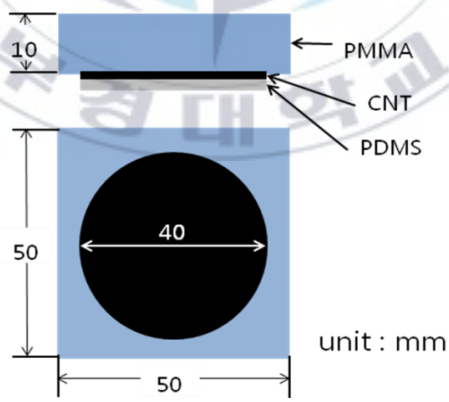

Fig. 3-5 Structure of the fabricated CNTs optoacoustic transducer. The diameter of the circular CNT/PDMS film is 40 mm. The size of the PMMA substrate is $50 \times 50\ mm^2$, and the thickness is 10 mm.

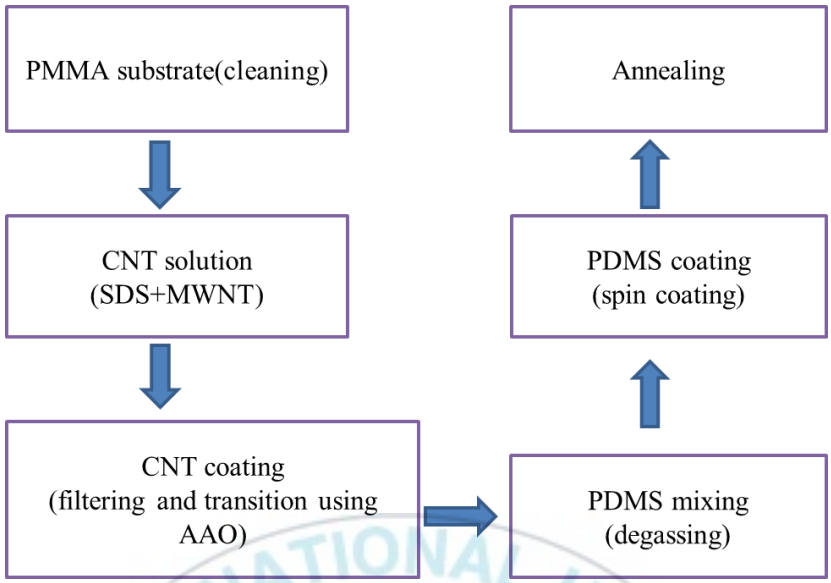

Fig. 3-6 Block diagram of the fabrication process of the optoacoustic transducer. The CNT film was coated on the PMMA substrate using vacuum filtration method. The PDMS film was coated on the surface of the CNT film using spin coating method.

In the fabrication of the CNT/PDMS optoacoustic transducers, the vacuum filtration method was used. Fig. 3-6 shows the block diagram of the fabrication process of the optoacoustic transducer. The PMMA substrate with the size of 50 mm × 50 mm, and thickness of 10 mm was prepared and cleaned using degassed water. In the fabrication of the optoacoustic transducer, a circular CNT film was formed by the vacuum filtration and transition method [48] using a multi-walled-CNT solution (0.1 wt% CNTs in 2.0 wt% sodium dodecyl sulfate water solution) and an anodic aluminum oxide (AAO) filter with a pore size of 0.2 μm. The diameter of the fabricated CNT film were about 40 mm. Then, the CNT film was attached onto the surface of the rectangular PMMA substrate and put into the oven (temperature: 50 ℃) to make the CNT film well attached for 30 minutes. Thereafter, PDMS (Dow Corning Sylgard 184)

was coated on the surface of the CNT film using spin coating method after degassing [49]. The thickness of the CNT and PDMS were changed by the amount of the CNT solution and the iteration number of spin-coating, respectively. During the spin coating process, PDMS permeates through the CNT film and forms a CNT/PDMS composite [50, 51]. Finally, the CNT/PDMS optoacoustic transducer was put into the oven (temperature: 120 ℃) to make the spin coated PDMS dry homogeneously.

CNT coating procedure using vacuum filtration method:

- Disperse MWNT in aqueous solution of surfactant SDS (Sodium Dodecyl Sulfate). The SDS used here is an aqueous solution having a weight ratio of 2%, and the MWNT added thereto is 0.1% by weight with respect to the aqueous solution.
- Pass the MWNT dispersion through AAO (Anodic Aluminum Oxide) filter. At this time, carbon nanotubes are caught in the filter, and a carbon nanotube film is formed on the filter.
- Place the filter with the carbon nanotube film in an aqueous solution of sodium hydroxide. The AAO filter is dissolved by the aqueous solution and the carbon nanotube film floats on the aqueous solution.
- Pour the dried carbon nanotube film over the PMMA substrate and dry it.

PDMS coating procedure using spin coating method:

- Mix the elastomeric PDMS (SYLGARD 184) and the curing agent in a weight ratio of 10: 1 using a glass rod in air.
- Degassing for 30 minutes in a vacuum chamber of approximately Torr.

- The prepared solution was coated on the coated CNTs and spin-coated. At this time, the sample was subjected to a first low-speed rotation at about 600 rpm for 30 seconds, and then a second high-speed rotation was performed at about 5000 rpm for 3 minutes.
- Heat treatment is then carried out in a thermostatic chamber at 100 ° C for 1 hour.

Table 3-2 Thickness of CNT films and PDMS films of the fabricated optoacoustic transducers.

No.	CNT film Thickness (μm)	PDMS film Thickness (μm)
1	0.3	4.5
2	0.7	4.5
3	1.4	4.5
4	0.7	4.5
5	0.7	9.0
6	0.7	13.5

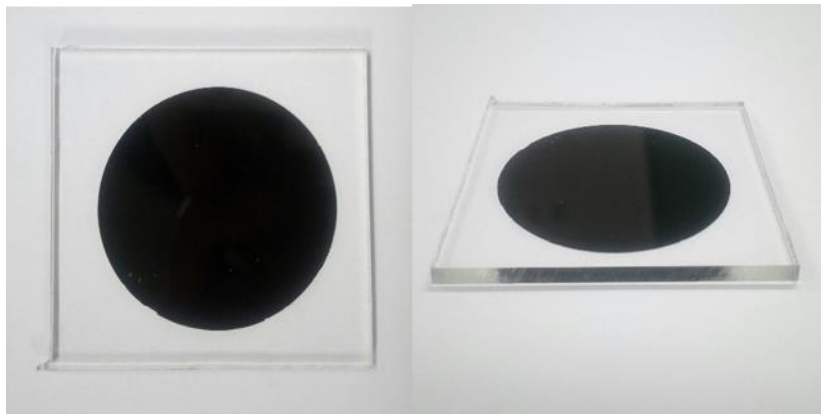

Fig. 3-7 Photograph of the fabricated CNT/PDMS optoacoustic transducer with PMMA substrate.

Table 3-2 shows the information of fabricated CNT/PDMS optoacoustic transducers with different thickness of CNT film and PDMS film. Among them, three transducers have the same 4.5μm thickness of PDMS film, while the thickness of the CNT films are 0.3 μm, 0.7 μm, 1.4 μm, respectively. The other three transducers have the same 0.7μm thickness of CNT film, while the thickness of the PDMS films are 4.5 μm, 9 μm, 13.5 μm, respectively. The thickness of the CNT films and PDMS films are measured using a surface profiler (Profilometer Alpha-Step). Fig. 3-7 shows the photograph of the fabricated CNT/PDMS optoacoustic transducer. And Fig. 3-8 shows the examples of thickness measurement of CNT film (0.7 μm) and PDMS film (4.5 μm) using the surface profiler (Profilometer Alpha-Step).

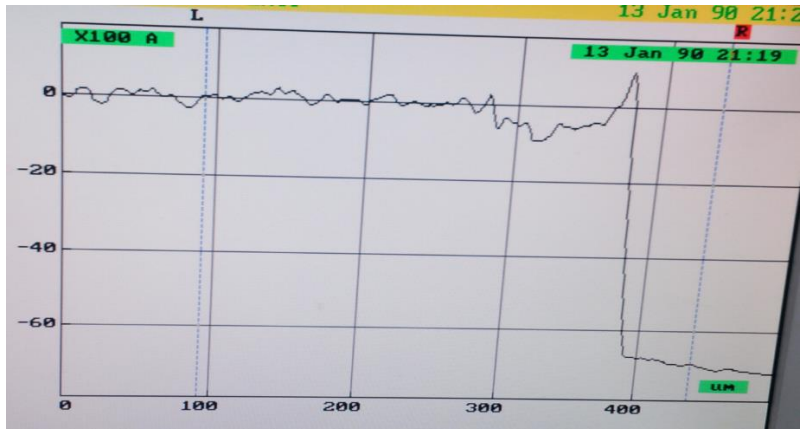

(a)

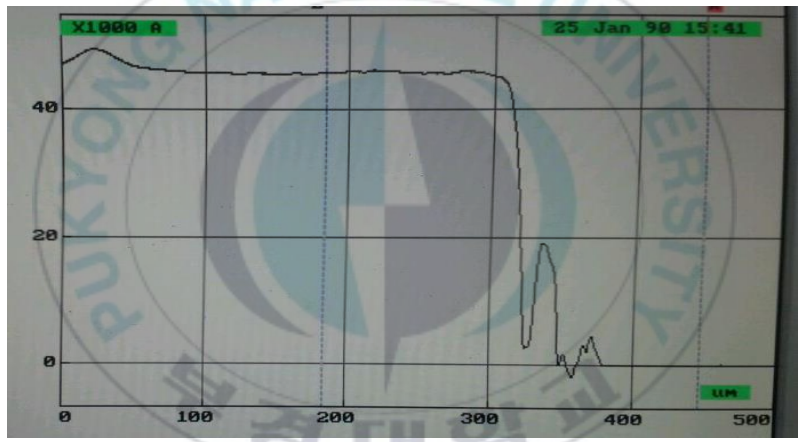

(b)

Fig. 3-8 Examples of thickness measurement of CNT film (0.7 μm) (a) and PDMS film (4.5 μm) (b) using a surface profiler (Profilometer, Alpha-Step).

(2) Fabrication process of the optoacoustic transducer with PET substrate

In the fabrication of the optoacoustic transducer with PET substrate, the materials and methods were same as that in the optoacoustic transducer with PMMA substrate. The only difference is material of substrate. In the fabrication, multi-walled CNTs and PDMS were coated on the surface of a PET sheet of 100 μm thickness and 50×50 mm^2 area by a vacuum filtration/transition method and a spin-coating method, respectively [48, 49]. As shown in Fig. 3-9, the diameter and thickness of the CNT/PDMS composite layer of the fabricated transducer were about 38 mm and 20 μm, respectively. Fig. 3-10 (a) shows the photograph of the fabricated CNT/PDMS optoacoustic transducer with PET substrate. Fig. 3-10 (b) shows the microscopy image showing thickness of each layer. The total thickness of the transducer was about 120 μm and the transducer was flexible.

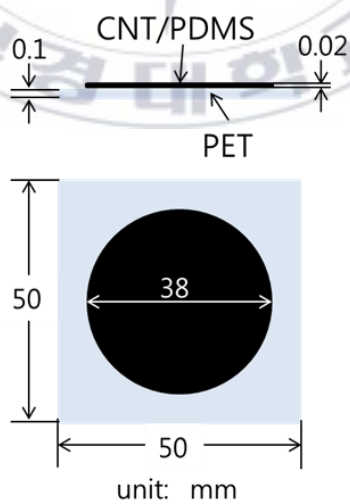

Fig. 3-9 Structure of the CNT/PDMS film transducer with PET substrate.

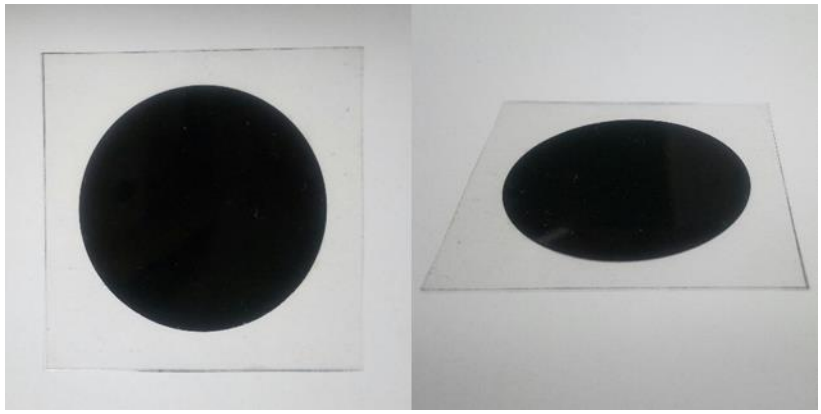

(a)

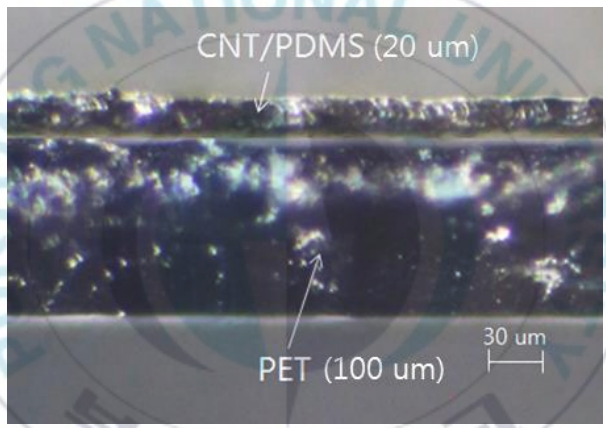

(b)

Fig. 3-10 Photograph of the fabricated CNT/PDMS optoacoustic transducer with PET substrate (a). Microscopy image showing thickness of each layer (b).

3.4. Summary

The CNT/PDMS optoacoustic transducer were fabricated by coating CNT film and PDMS film on a PMMA substrate and PET substrate using vacuum filtration method and spin coating method, respectively.

Ch. 4. Characteristics of ultrasound waves by the CNT/PDMS optoacoustic transducers

In this chapter, the characteristics of the generated ultrasound waves from the CNT/PDMS optoacoustic transducers when irradiated pulsed laser beams are investigated. Then, the propagation characteristics and acoustic fields of the generated ultrasound waves are measured and simulated.

4.1. Characteristics of the generated ultrasound

When the CNT/PDMS optoacoustic transducer was irradiated by pulsed laser beams, the laser energy was absorbed by the CNT/PDMS film resulting in a region of higher temperature. The rise in temperature generated an expanding region and ultrasound waves were generated because of the optoacoustic effect. The waveform of the generated ultrasound waves was investigated

4.1.1. Experiment

Figure 4-1 shows a schematic diagram of the experimental setup for measurement of the generated ultrasound by the CNT/PDMS optoacoustic transducer. A Q-switched Nd:YAG laser (Quanta-Ray, Spectra-Physics Inc.) with 532 nm wavelength and about 8 ns pulse width was used as a light source. The laser can radiate maximum 160 mJ per pulse with 20 Hz PRF. To make parallel beam with maximum 40 mm diameter, the laser beam was expended by a lens (NT55-582, Edmund Ltd.) after passing an iris. It was collimated by a plano-convex lens with 50 mm diameter and 36 mm focal length. The illuminated area could be changed by the iris and the laser power was measured by a

power meter (PM100D, Thorlabs Inc.) with a detector (S370C, Thorlabs Inc.).

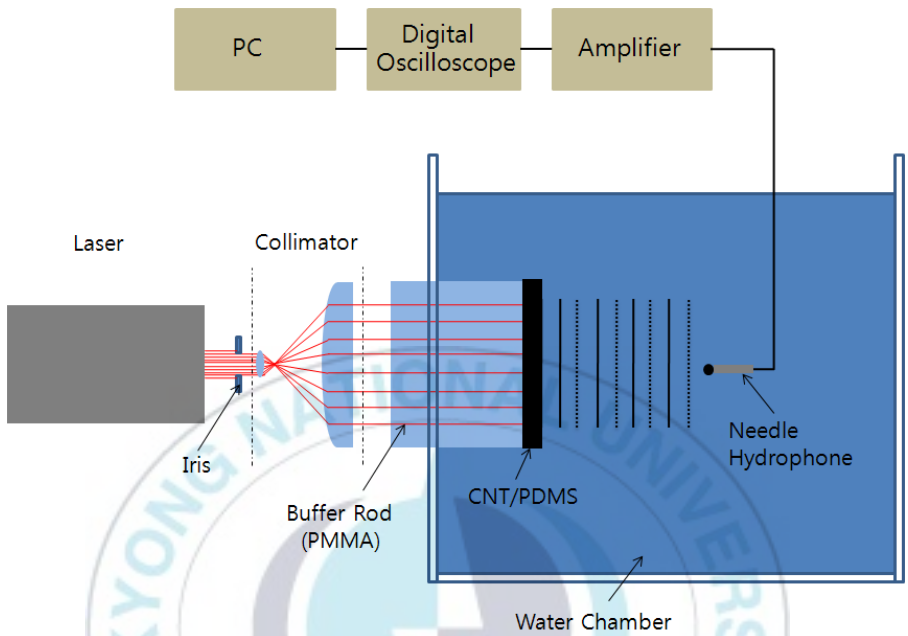

Fig. 4-1 Schematic of experimental setup for measurement of the generated ultrasound by the CNT/PDMS optoacoustic transducer. A Q-switched Nd:YAG laser (Quanta-Ray, Spectra-Physics Inc.) with 532 nm wavelength and about 8 ns pulse width was used as the light source.

The CNT/PDMS optoacoustic transducer was irradiated by the laser source and the laser energy was absorbed by the CNT/PDMS film resulting in a region of higher temperature. The rise in temperature generated an expanding region and ultrasound waves propagated away from the heated surface of the CNT/PDMS film. The generated ultrasound waves were measured using a commercial PVDF needle hydrophone (Φ=0.2 mm, Precision Acoustics) with an 8 dB preamplifier in water. The dimensions of the water chamber were $10(\mathrm{H}) \times 20(\mathrm{W}) \times 50\ (\mathrm{L})\mathrm{cm}^3$ and the measurement position was

controlled using an x-y-z step motor. The measured ultrasound waves were displayed in an oscilloscope (Lecroy LT322) and the data were saved to a PC.

4.1.2. Results

When the laser beams irradiated on the surface of the CNT/PDMS optoacoustic transducer, the ultrasound waves were generated. Fig. 4-2 (blue color waveform) shows the generated ultrasound waves measured by the commercial PVDF needle hydrophone. The red dash waveform shows the typical waveform of the blast wave-like shock wave fitted by the following Friedlander equation [52].

$$\mathrm{p} = p_0\left(1 - \frac{t-t_0}{T_0-t_0}\right)\exp\left(-\frac{t-t_0}{T_0-t_0}\right) \quad (4\text{-}1)$$

Here, p_0 is the peak pressure, and t_0 and T_0 are the time when the shock wave begins and the time when the pressure first becomes zero before the pressure becomes negative, respectively. The waveforms are similar to those produced by extracorporeal shock wave lithotripsy in a focal region [53, 54] and those in Ref [55]. Fig. 4-2 shows that the waveform and spectra can be fitted well by Eq. (4-1) with p_0 = 2.91 MPa, t_0= 13.33 μs, and T_0= 13.37 μs. It is shown that the generated ultrasound waves have the waveform of the blast wave-like shock wave. It indicates that the generated ultrasound waves by the CNT/PDMS optoacoustic transducer are shock waves.

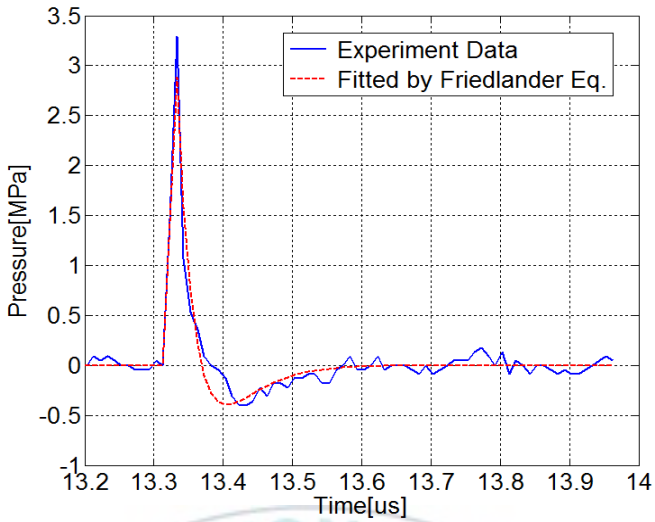

Fig. 4-2 Comparison of measured typical waveform with calculated one by Friedlander equation. The results shows that the generated ultrasound waves from the CNT/PDMS coated plane optoacoustic transducers are shock waves.

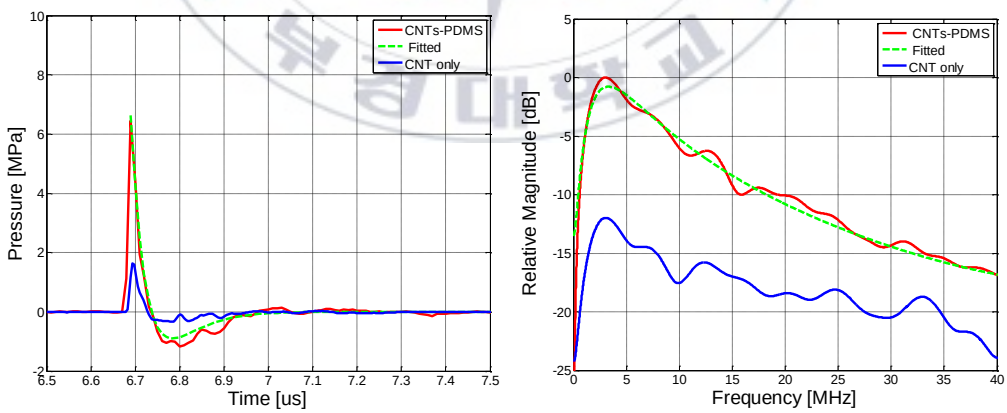

(a) (b)

Fig. 4-3 Comparison of the waveforms (a) and spectra (b) between the transducers with and without PDMS coating.

Figure 4-3 shows the comparison of the waveforms and spectra of the measured shock waves. The peak pressure of the shock wave by the CNT/PDMS optoacoustic transducer is more than three times higher than that of the shock wave by the CNT coated only transducer. The PDMS has a high thermal coefficient of volume expansion, $0.92 \times 10^{-3}\ K^{-1}$, which is 4.5 fold higher than water ($0.21 \times 10^{-3}\ K^{-1}$). This means that, as soon as the CNT film are heated by the light absorption, they give out most of the thermal energy to the surrounding PDMS film which can cause instantaneous thermal expansion with high amplitudes.

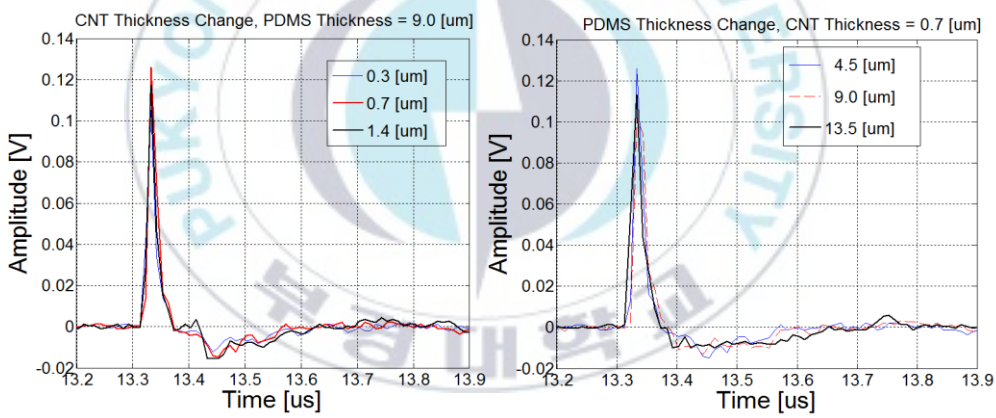

(a) (b)

Fig. 4-4 Measured waveforms (a) according to CNT film thickness when the PDMS film thickness is 9.0 μm, and the waveforms (b) according to PDMS thickness when the CNT thickness is 0.7 μm. All of the waves have the similar waveform as blast wave-like shock waves.

It is uncertain whether the thickness of the CNT film and PDMS film affect the waveform and peak magnitude of the generated shock waves or not. In order to confirm the problem, the related experiments were completed using CNT/PDMS optoacoustic transducers with different thickness of CNT films and PDMS films. Fig. 4-4(a) shows the measured waveforms of the generated shock waves when the PDMS film thickness is 9.0 μm while the thickness of CNT films are 0.3 μm, 0.7 μm, 1.4 μm, respectively. Fig. 4-4(b) shows the measured waveforms of the generated shock waves when the thickness of CNT film is 0.7μm, while the thickness of PDMS films are 4.5 μm, 9 μm, 13.5 μm, respectively.

Fig. 4-4 shows that all of the measured ultrasound waves have the similar waveform as blast wave-like shock waves when the thickness of the CNT film and PDMS film changes. It is once again confirmed that the generated ultrasound waves by the CNT/PDMS optoacoustic transducer are shock waves. It is noted that the measured shock waves have maximum peak magnitude in the two groups when the thickness of CNT film and PDMS film are 0.7μm and 4.5μm, respectively. However, among the results, the maximum peak magnitude was obtained when the thickness of CNT film and PDMS film are 0.7μm and 9.0μm, respectively. In the next experiments, the CNT/PDMS optoacoustic transducers with the thickness of CNT film and PDMS film are 0.7μm and 9.0μm, respectively, were used to measure other characteristics.

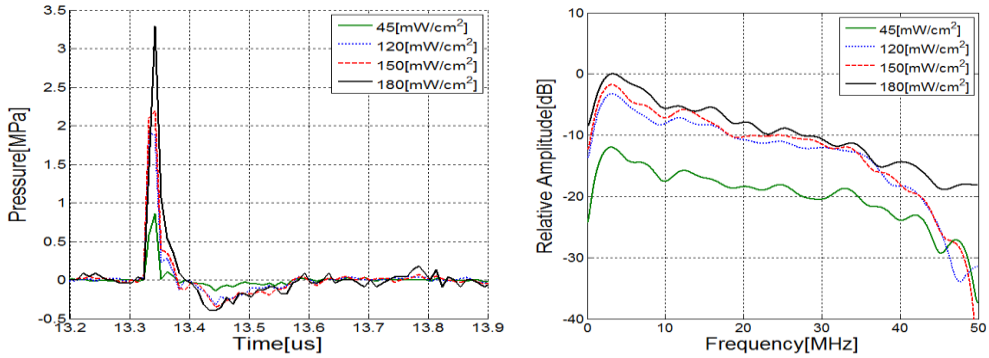

(a) (b)

Fig. 4-5 Variation of waveforms (a) and power spectra (b) with laser intensity. It is noted that the pressure waves vary with the laser intensity, but all of them keep the waveform of blast wave-like shock waves.

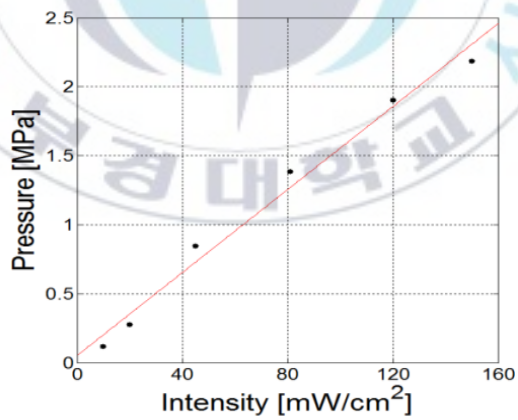

Fig. 4-6 Variation of the peak pressure with laser intensity. It is noted that the peak amplitude of the waves linearly varies with the laser intensity.

Figure 4-5 shows the variation of waveforms and power spectra of the measured shock waves generated by the CNT/PDMS optoacoustic transducer. When the laser intensity increased from 45 mW/cm^2 to 180 mW/cm^2, the peak acoustic pressure of the measured shock waves also increased from 0.85 MPa to 3.36 MPa. It is noted that the pressure waves vary with the laser intensity, but all of them keep the waveform of blast wave-like shock waves. Fig. 4-6 shows that the magnitude of the peak pressure of the generated shock waves varied with the laser intensity linearly.

Figure 4-7 and Fig. 4-8 show the variation of the generated shock waves along axial (X-axis) and lateral (Y-axis) distances, respectively. The generated shock waves were measured with the step size 2 mm and total distance 22 mm using a step motor. In the axial direction, the maximum magnitude of the generated shock waves is the one measured close to the surface of the CNT/PDMS optoacoustic transducer, which is about 80 mV. The magnitude decreases when the detected point moved away from the transducer surface along the axial distance. In the lateral direction, the generated shock waves at the central part have the biggest magnitude, while the magnitude decreases when measurement away from the center point. In Fig.4-8, one shock wave at the central part has smaller peak magnitude compared to the other ones. It is because the laser intensity is not homogenous.

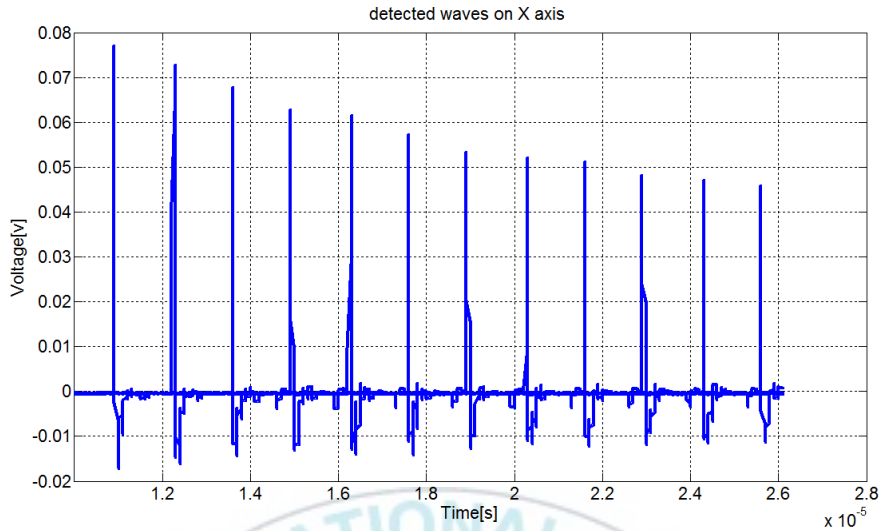

Fig. 4-7 Detected waves along axial (X-axis) distance with step size of 2 mm and total distance of 22 mm. The peak magnitude decreased along the axial distance.

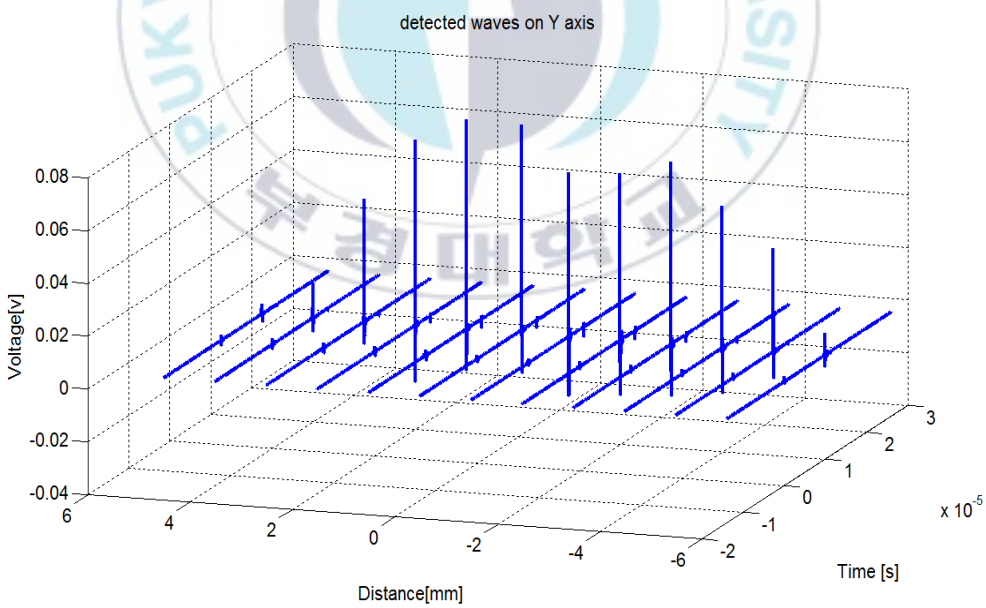

Fig. 4-8 Detected waves along lateral (Y-axis) distance with step size of 2 mm and total distance of 22 mm. The shock waves at the central point has the maximum magnitude because the laser beam is not homogenous.

4.2. Propagation characteristics of the generated shock waves

Because of the high efficiency of optical energy absorption and high thermal conductivity of the CNT film and high thermal coefficient of volume expansion of the PDMS film, ultrasound waves were generated when the CNT/PDMS optoacoustic transducer was irradiated a pulsed laser. The generated ultrasound wave has a waveform of blast wave-like shock wave. Some propagation characteristics of the planar shock waves from the fabricated CNT/PDMS optoacoustic transducer were measured and compared with the calculated results.

4.2.1. Experiment

Figure 4-9(a) shows a schematic diagram of the experimental setup for measure the propagation characteristics of the shock waves generated from the CNT/PDMS optoacoustic transducer. A Q-switched Nd:YAG laser (Spectra-Physics Quanta-Ray) of 532 nm wavelength and 8 ns pulse width, with a maximum of 160 mJ/pulse and 20 Hz PRF, was used as the light source. The radiated laser beam was expanded and collimated by two lenses. Laser power was measured using a power meter (Thorlabs PM100D) and a detector (Thorlabs S370C). The generated ultrasound waves were measured using a needle hydrophone ($\Phi = 0.2$mm, Precision Acoustics) with an 8 dB preamplifier in water. The dimensions of the water chamber were $10(\mathrm{H}) \times 20(\mathrm{W}) \times 50\ (\mathrm{L})\mathrm{cm}^3$ and the measurement position was controlled using an x-y-z step motor. The measured ultrasound waves were displayed and saved by the PXI (National Instrument).

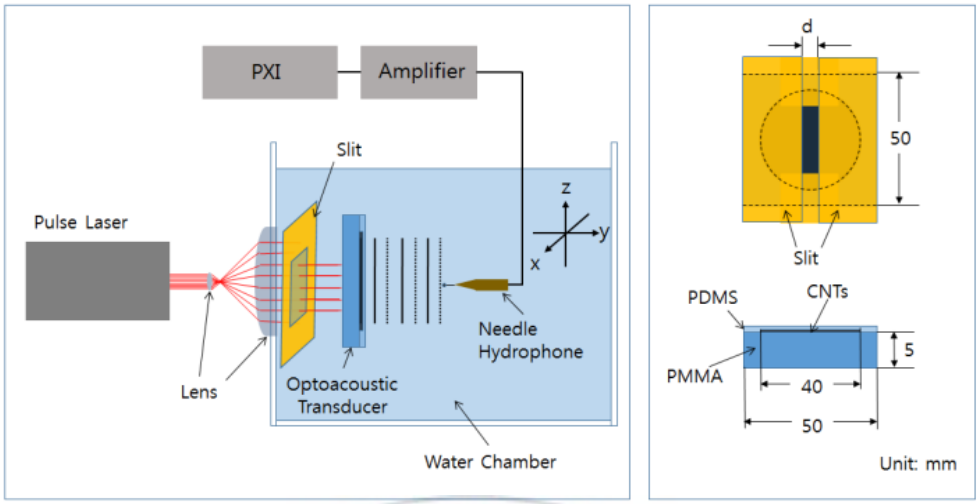

(a) (b)

Fig. 4-9 Schematics of experimental setup (a) and structure of the transducer with a slit (b).

4.2.2. Results

Propagation speed

When the laser beams irradiated on the surface of the CNT/PDMS optoacoustic transducer, the ultrasound waves were generated. Fig. 4-10 shows the typical waveforms and spectra of ultrasound waves generated from the CNT/PDMS optoacoustic transducers measured by the commercial PVDF needle hydrophone. These waves were measured about 10 mm away from the surface of the transducer when it was illuminated at a laser power of 120 mJ/pulse. It is shown that the generated ultrasound waves have the typical waveform of the blast wave-like shock wave, which can be described by the following Friedlander equation (Eq. 4-1) [52]. Fig. 4-10 shows that the waveform and spectra can be fitted well by Eq. (4-1) with p_0 = 6.35 MPa, t_0= 6.67 μs, and T_0= 6.74 μs.

To investigate the sound speed variation according to propagation, the time delay for a 0.1 mm movement was measured using a 500 MHz digital oscilloscope (Tektronix MSO/DPO2000B) in the range of 10.0 to 60.0 mm from the surface of the transducer. The sampling time resolution of the oscilloscope was 10 ns. The delay time was obtained from the times of two start points of the detected shock waves in the oscilloscope. Because of the time resolution, it might have $\pm$10 ns error in the starting points. Fig. 4-11 shows the results in water at 24.5 ℃. There was no significant dependence on propagation distance within the given range. The wave propagation speed was determined to be 1505.3 m/s from the average delay time of 66.433 ns. Even though it may have a large error, the propagation speed is meaningful because it was obtained from the average of 500 data. The speed is higher than the usual sound speed

of 1495.7 m/s, which was estimated using an empirical equation [56].

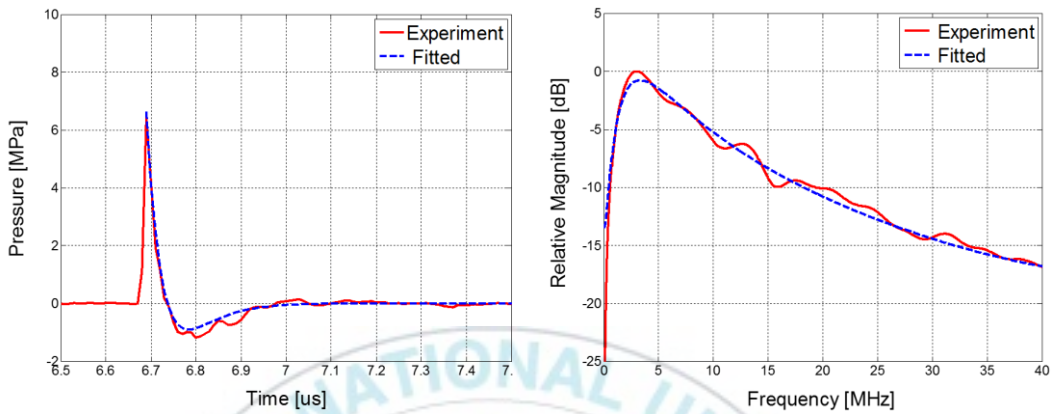

(a) (b)

Fig. 4-10 Waveform (a) and spectra (b) of the shock waves from the CNT/PDMS optoacoustic transducer.

Figures 4-12(a) and 4-12(b) show the variations of waveforms and peak pressure with propagation distance, respectively. The waveforms of shock waves did not change markedly. By fitting it, an attenuation coefficient of 0.24 dB/cm was obtained, which corresponds to the absorption of a 10.5 MHz harmonic plane wave if we deduce it from $25.3\times10^{-17}/f^2$ Np/cm [57]. However, the frequency of the maximum pressure is 3.05 MHz, as shown in Fig. 4-10(b). This means that the attenuation of this blast wave is more significant than that of an ordinary small-amplitude pulse wave with the same center frequency.

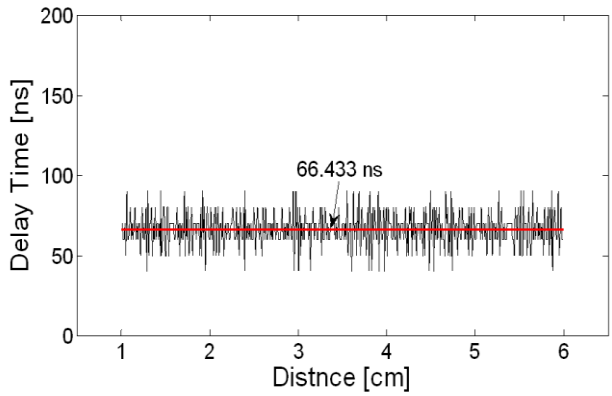

Fig. 4-11 Delay time for 0.1 mm movement in the range of 10 to 60 mm.

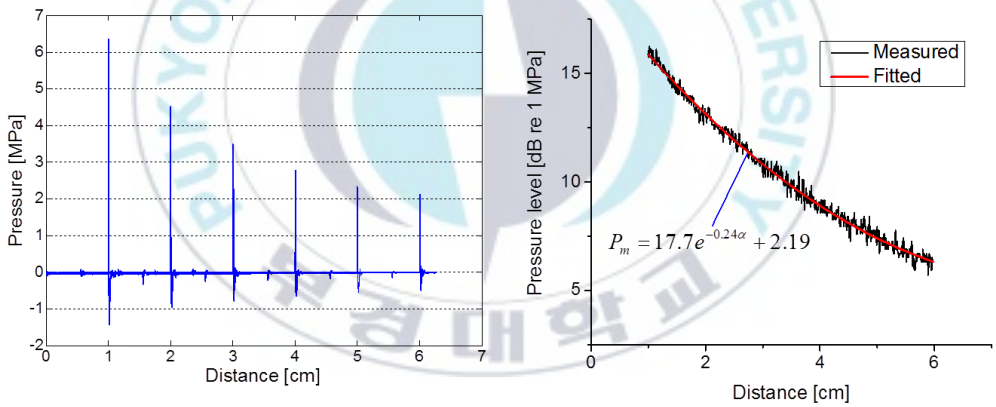

(a) (b)

Fig. 4-12 Variation of the waveform (a) and peak pressures (b) in the range of 10 to 60 mm.

Acoustic fields

To confirm whether the transducer radiates planar shock waves, we investigated two-dimensional pressure fields. The region to be illuminated homogenously by the laser beam on the transducer surface was selected using a rectangular slit, as shown in Fig. 4-9(b). First, the fields were calculated numerically by the FFT method. In this method, the surface is divided into many point sources and every source generates the same shock wave, as given by the Friedlander equation. It is assumed that the peak pressure on the transducer surface is 10.0 MPa.

The calculated and measured static pressure fields for the surface with the length $l = 10$ mm and the width $d = 3.0$ mm or 5.0 mm are shown in Fig. 4-13(a) and 4-13(b). The figures show that the calculated peak pressures are higher than the measured ones. This is because any other effects, such as absorption, were not considered in the calculation. Moreover, owing to the inhomogeneity and diffraction of the laser beam as it pass through the slit, there are some differences between the calculated and the measured field patterns, especially for the 3 mm slit. However, it is clearly revealed that the fields are simply changed without any significant interference pattern or side lobes. The measurement and calculated results are relatively well matched in that respect.

From the comparison of results, it is noted that the surface vibrated like a piston transducer with the same phase, which could radiate planar waves. In Fig. 4-14, the simulation results of transient fields obviously show that the propagating wave has a planar wave front within the vibrating region, especially near the transducer.

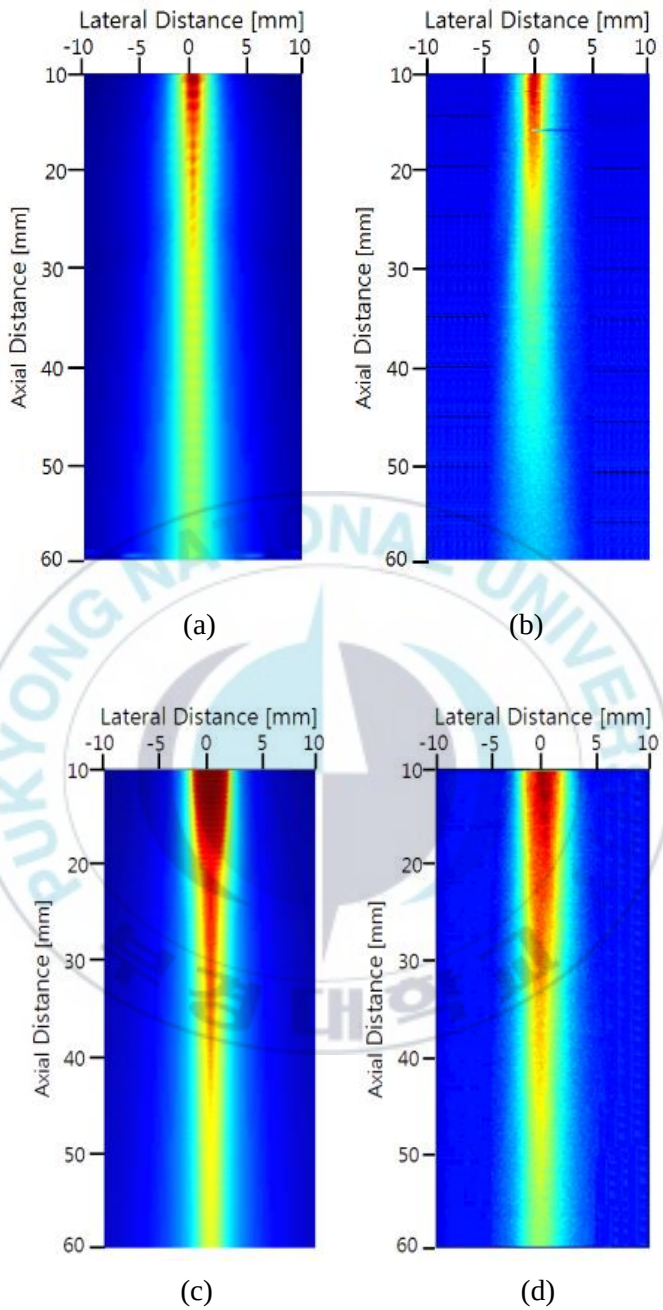

Fig. 4-13 Two-dimensional peak pressure fields when the transducer illuminated through a slit: calculated (3 mm) (a), measured (3 mm) (b), calculated (5 mm) (c), and measured (5 mm) (d).

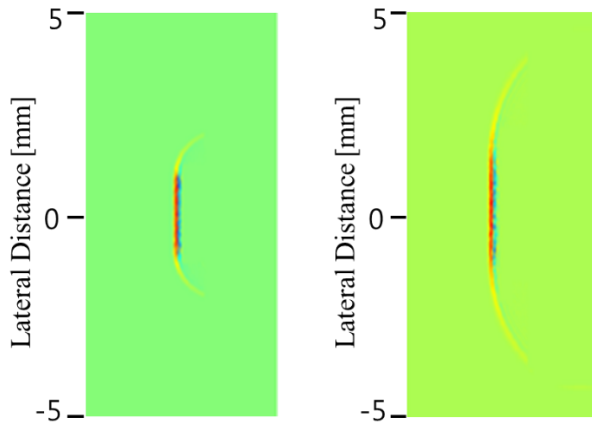

(a) (b)

Fig. 4-14 Transient wave fronts of the shock wave when they propagated 13 mm from the transducer through a slit: 3 mm (a) and 5 mm (b).

4.3. Summary

It is demonstrated that the generated ultrasound waves from the CNT/PDMS optoacoustic transducers when irradiated pulsed laser have the blast wave-like shock waves which could be fitted well by Friedlander equation. The spin coated PDMS film has great influence on the peak pressure of the generated shock waves. However, the waveform doesn't have any significant dependence on the CNT film or the PDMS film thicknesses in the given range.

The propagation characteristics of the generated ultrasound waves, including sound speed and the attenuation coefficient of the blast waves in water, were measured. From the comparison between the measurement and calculation of two-dimensional acoustic pressure fields, it is demonstrated that the generated ultrasound waves are planar shock waves.

Ch. 5. Confirmation of the shock waveform by the CNT/PDMS optoacoustic transducers using NDT transducers

Owing to the optoacoustic effect, a composite of light-absorbing and elastomeric materials can generate ultrasound waves when it is illuminated by a pulse laser. However, the waveform of the generated ultrasound waves by the optoacoustic transducers have not been intensively investigated so far. In Ch. 4, it is shown that the measured waves from an optoacoustic plane transducer made of CNT/PDMS composite, which were coated on a poly(methyl methacrylate) (PMMA) substrate, have blast wave-like waveforms. Those ultrasound waves were measured by a commercial PVDF needle hydrophone or an optical fiber hydrophone. Each hydrophone has wideband characteristics so that the receiving response is flat in the frequency range from the several hundred kHz to the several hundred MHz. But, it has low sensitivity and the skill is necessary to calibrate it well. Furthermore, it is easily damaged and the price is expensive. On the other hand, the NDT transducers have high sensitivity and are robust. Those are widely and practically used in industry because of low price compare to the PVDF needle hydrophones or optical fiber hydrophones.

In this chapter, the shock waveform of the generated ultrasound by the CNT/PDMS optoacoustic transducer was measured and confirmed using NDT transducers with narrow bandwidth considering the receiving impulse responses of the transducers. The waveforms of the shock waves were simulated using the PiezoCAD (Version 3.03 for windows, Sonic concepts, Wood-in-ville, WA), and the results were compared with measured ones by a commercial PVDF needle hydrophone and an optical fiber

hydrophone.

5.1. Theory

Pulse-echo response

The pulse echo method is a very useful technique for nondestructive testing. It could be used to measure the velocity, wavelength and attenuation coefficient (damping constant) of acoustic waves. It is also a useful method to evaluate the characteristics of ultrasound transducers.

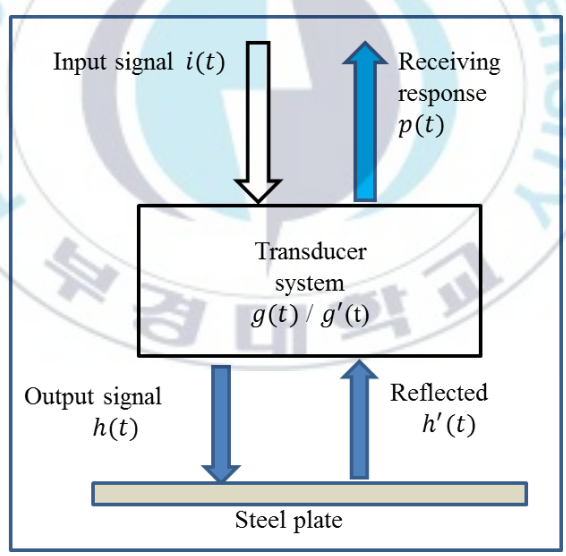

Fig. 5-1 Schematic diagram for the theory of pulse echo measurement.

Table 5-1 Meanings of the parameters in the schematic diagram for the theory of pulse echo measurement.

Parameters	Meaning
$i(t)$	Driving pulse from the Pulse/Receiver, input signal
$g(t)$	Transmitting impulse response of the transducer system
$h(t)$	Transmitted waves from the transducer, output signal
$h'(t)$	Reflected waves from the steel reflector
$g'(t)$	Receiving impulse response of the transducer system
$p(t)$	Receiving response by the Pulse/Receiver
$f(t)$	Generated ultrasound waves by the CNT/PDMS transducer
$r(t)$	Measured waves with the receiving response

Figure 5-1 shows the schematic diagram for the theory of pulse echo measurement. The input pulse signal $i(t)$ generated from a Pulse/Receiver equipment drives a NDT transducer system which has the impulse response $g(t)$. Here the NDT transducer system includes the electrical impedance matching circuit and cables for the connection of the transducer. Then the transmitting wave $h(t)$ from the NDT transducer is reflected from the surface of a reflector, a steel plate is used in this study. The reflected wave is $h'(t)$. The NDT transducer system which has the receiving impulse response $g'(t)$ receives the reflected wave $h'(t)$, and the Pulse/Receiver finally shows the receiving response $p(t)$. The equations related to the measurement are summarized as below:

$$h(t) = i(t) * g(t)\,, \tag{1}$$

here, $'*'$ means the convolution.

$$h'(t) = R \cdot h(t) \tag{2}$$

R is the reflection coefficient on the water/steel plate boundary.

$$p(t) = h'(t) * g'(t) \tag{3}$$

From Eq. (1), (2), and (3),

$$p(t) = R \cdot i(t) * g(t) * g'(t) \tag{4}$$

By the Fourier transform and convolution theorem,

$$P(\omega) = R \cdot I(\omega) \cdot G(\omega) \cdot G'(\omega) \tag{5}$$

Because of the reciprocity of piezoelectric transducer,

$$G(\omega) = G'(\omega) \tag{6}$$

Then, the frequency response of the system is given by,

$$G(\omega) = [P(\omega)/(R \cdot I(\omega))]^{1/2} \tag{7}$$

Receiving response

Here, the receiving response is related to the waves by the NDT transducer generated from the CNT/PDMS optoacoustic transducer. Fig. 5-2 shows the schematic diagram for the theory of receiving response measurement. The generated ultrasound waves $f(t)$ from the CNT/PDMS optoacoustic transducer is detected by the NDT transducer system $g'(t)$. And the measured wave $r(t)$ is saved in a computer. Here are the equations in the receiving response measurement system:

$$r(t) = f(t) * g'(t) \tag{8}$$

From the Fourier transform and convolution theorem,

$$R(\omega) = F(\omega) \cdot G'(\omega) \tag{9}$$

Then,

$$F(\omega) = R(\omega)/G'(\omega) \tag{10}$$

From Eq. (7),

$$F(\omega) = R(\omega) \,/\, [P(\omega) \,/(R \cdot I(\omega))]^{1/2} \tag{11}$$

Then, with the inverse Fourier transformation, the received signal is given by,

$$f(t) = F^{-1}\,[\,F(\omega)\,] = F^{-1}\,[\,R(\omega) \,/\, [P(\omega) \,/\, (R \cdot I(\omega))]^{1/2}\,] \tag{12}$$

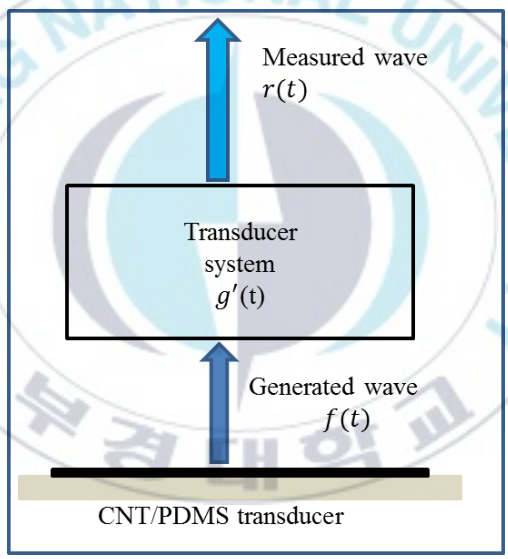

Fig. 5-2 Schematic diagram for the theory of receiving response measurement.

5.2. Materials

Figure 5-3(a) shows the structure of the fabricated CNT/PDMS optoacoustic transducer. Fig. 5-3(b) shows the photograph of the two NDT transducers used in this experiment. Table 5-2 shows the parameters of the two NDT transducer. Both of the

NDT transducers have circle shapes and same center frequencies but with different element sizes.

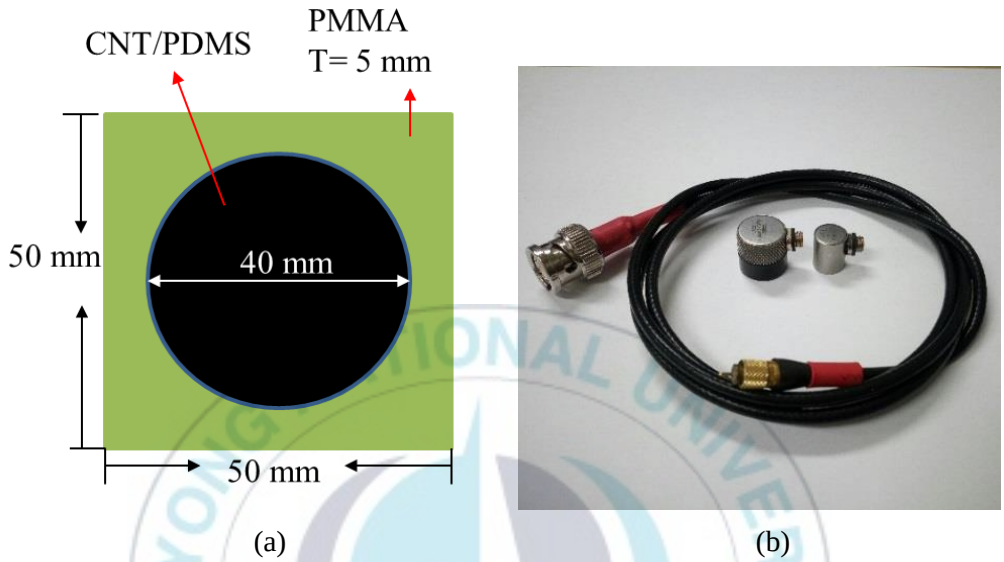

Fig. 5-3 Structure of the fabricated CNT/PDMS optoacoustic transducer (a), and photograph of the two NDT transducers (b).

Table 5-2 Parameters of the two NDT transducers.

Parameter	NDT-1	NDT-2
Element size (diameter)	9.53 mm	6.35 mm
Center frequency	7.5 MHz	7.5 MHz

5.3. Experiment

Figure 5-4 shows the schematics of experiment setup for measurement of the pulse echo impulse response. The size of the water chamber is 10 cm × 10 cm × 10 cm. The steel plate was used as the reflector for pulse echo measurement. The NDT transducers

were excited by an electrical pulse signal generated by a Pulse/Receiver equipment (Panametrics 5800). And the reflected ultrasound wave from the steel plate was also received by the Pulse/Receiver equipment. Table 5-3 shows the parameter setting of the Pulse/Receiver for pulse echo measurement of the NDT transducers. The detected ultrasound wave was displayed and saved by an oscilloscope (LeCroy LT322). During measurement, the NDT transducers were fixed and moved by an x-y moving step motor.

Table 5-3 Pulse/Receiver conditions for pulse echo measurement.

Parameters	**Setting value**
Pulse frequency	1.0 KHz
Input energy	1 μJ
Voltage	100 V
Damping	50 Ω
Attenuation	0 dB
Gain	20 dB
Low pass filter	15 MHz
High pass filter	500 KHz

Figure 5-5 shows the schematics of experiment setup for measurement of the generated ultrasound waves from CNT/PDMS transducer. The experiment setup almost same as that in Fig. 5-4 while the steel plate was substituted with the CNT/PDMS optoacoustic transducer. The Q-switched Nd:YAG laser (Spectra-Physics Quanta-Ray) of 532 nm wavelength and 8 ns pulse width was used to irradiated the he CNT/PDMS optoacoustic transducer.

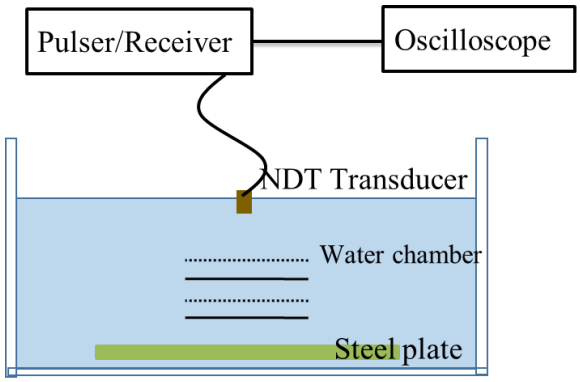

Fig. 5-4 Schematics of experiment setup to measure the pulse echo impulse response.

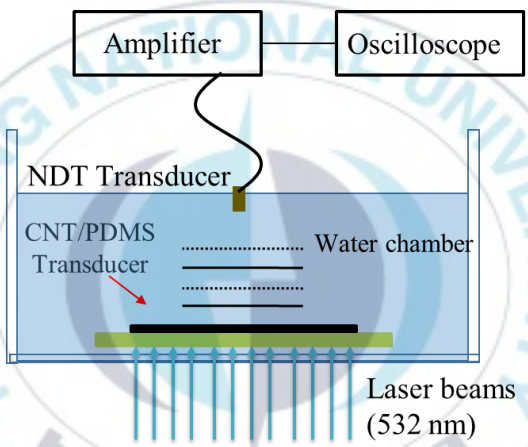

Fig. 5-5 Schematics of experiment setup to measure the generated ultrasound waves from CNT/PDMS transducer.

According to the measured pulse echo impulse response, the receiving impulse response of the NDT transducers was simulated using the PiezoCAD (Version 3.03 for windows, Sonic concepts, Wood-in-ville, WA). The math calculation for the Fourier transformation and the inverse Fourier transformation of the wave data were processed using Matlab (Version 2012a).

5.4. Results

Figure 5-6 shows the measured and simulated pulse echo impulse response using the Pulse/Receiver equipment and PiezoCAD software, respectively, of NDT-1 transducer. And Fig. 5-7 shows the measured and simulated pulse echo impulse response of NDT-2 transducer. The function of the PiezoCAD software was so powerful that the simulated waveforms and spectrums were similar to the measured ones when input the parameters same as that of the NDT transducers.

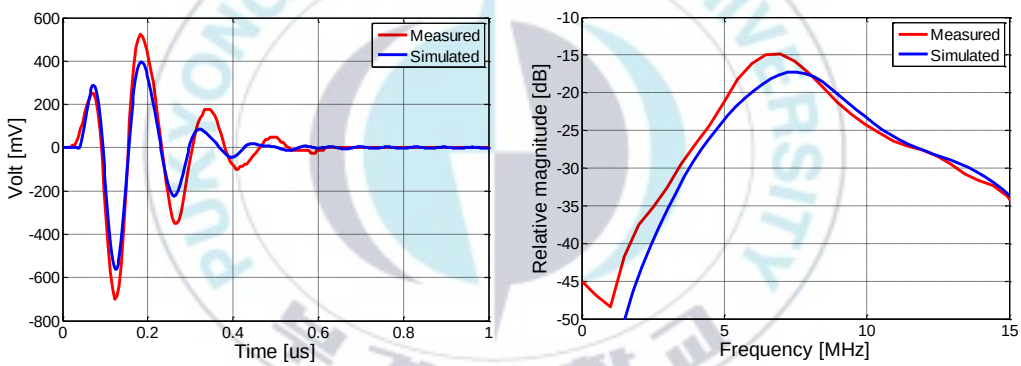

(a) (b)

Fig. 5-6 Measured and simulated pulse echo impulse response of NDT-1. Waveforms (a) and spectrums (b).

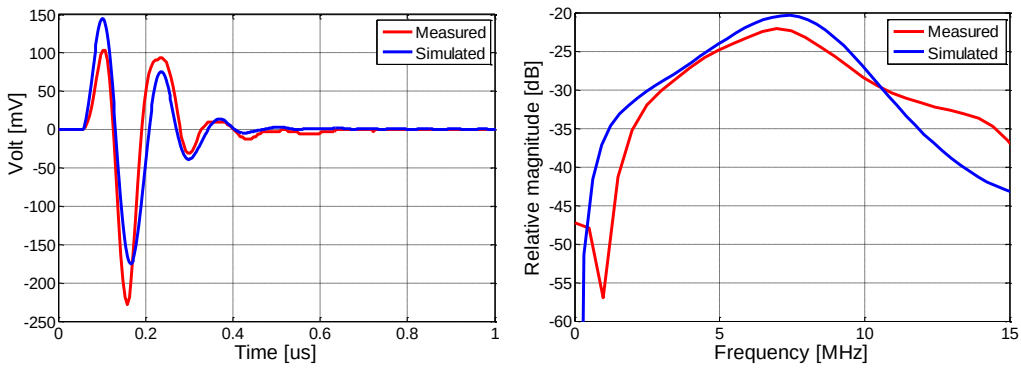

(a) (b)

Fig. 5-7 Measured and simulated pulse echo impulse response of NDT-2. Waveforms (a) and spectrums (b).

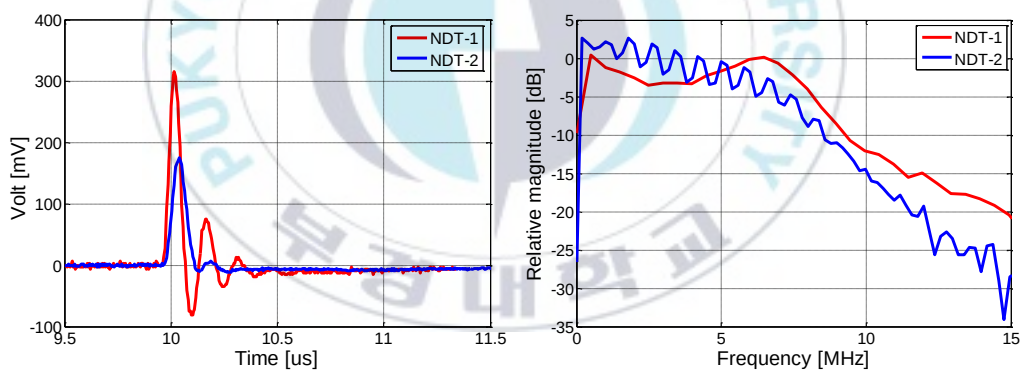

(a) (b)

Fig. 5-8 Measured waveforms and spectra by NDT transducers. (a) Waveforms and (b) spectrums.

Figure 5-8 shows the measured ultrasound waves generated by the CNT/PDMS optoacoustic transducers using the NDT-1 and NDT-2 transducers, respectively. With these measured wave data and the simulated ones from PiezoCAD, the math calculation

of the Fourier transformation and inverse Fourier transformation were processed using the Matlab software. Fig.5-9 shows the calculated waves from the characteristics of NDT-1 and NDT-2 transducers. The calculated waves were compared with the waves measured by the commercial PVDF needle hydrophone and the fiber optic transducer. It is shown that the calculated waves have the waveform of a blast wave-like shock wave, which is similar to the waveform of the shock waves measured by the commercial PVDF needle hydrophone and the fiber optic transducer.

The results confirmed that the generated ultrasound waves from the CNT/PDMS optoacoustic transducer when irradiated a pulsed laser are shock waves.

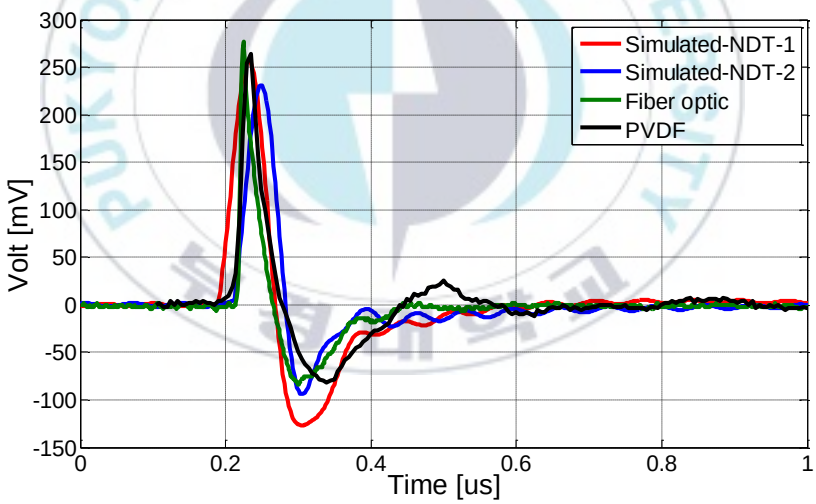

Fig. 5-9 Calculated waveforms of NDT transducers, and compared with the ones by the commercial PVDF needle hydrophone and fiber optic transducer.

5.5. Summary

By considering the receiving impulse responses, the waveforms of the generated ultrasound waves from the CNT/PDMS optoacoustic transducer were confirmed by using the NDT transducers with narrow bandwidth. It is confirmed that the generated ultrasound waves from the CNT/PDMS optoacoustic transducer have the blast wave-like waveforms as same as the waveforms by a PVDF needle hydrophone or optical fiber hydrophone. Conclusively, it is known that the ultrasound waves from the CNT/PDMS optoacoustic transducer can be measured by NDT transducers.

Ch. 6. Characteristics of the CNT/PDMS film optoacoustic transducers and their applications

Owing to the optoacoustic effect, a composite of light-absorbing and elastomeric materials generates ultrasound waves efficiently when it is illuminated by a pulse laser. Recently, ultrasound transducers with this effect and their applications have been intensively investigated [13, 55, 58]. To fabricate optoacoustic transducers, light-absorbing and elastomeric materials should be coated on a transparent substrate. A solid material such as glass has generally been used as the substrate so far [14, 59].

In Chapter 4 , an optoacoustic plane transducer made of carbon nanotubes (CNTs) and poly(dimethylsiloxane) (PDMS), which were coated on a poly(methyl methacrylate) (PMMA) substrate, can effectively generate shock waves [60, 61]. However, the acoustic pressure of the generated shock waves is not very high, it is only about 3MPa-7MPa. Even though the acoustic pressure could be increased by irradiating laser with high intensity on the optoacoustic transducer, the CNT/PDMS would be damaged and detached because of the radiation force by high laser energy. Focused transducers that are operated by low laser energy can generate high acoustic pressure near their focal point.

In this chapter, the shock wave generation and propagation characteristics of the CNT/PDMS film transducer fabricated by coating the composite of CNT/PDMS on the surface of a thin flexible optical poly(ethylene terephthalate) (PET) sheet was investigated. And, the characteristics was compared with the plane transducer made of the same CNT/PDMS film. Because the spin-coating method is suitable for a plane

substrate, it is difficult to make a focused transducer. Especially, to make a line-focused transducer is impossible. So that, as an application, the line-focused optoacoustic transducer with a cylindrical radiation surface was fabricated by using the film transducer in this study. A very high maximum pressure of about 35 MPa was obtained using the source. It was demonstrated that the source can engrave a line trace on a chalk surface.

6.1. CNT/PDMS optoacoustic transducers on PET film substrate

6.1.1. Experiment

Figure 6-1 shows a schematic diagram of the experimental setup. As the optical source, a Q-switched Nd:YAG laser of 532 nm wavelength and about 8 ns pulse width, with 11-499 mJ/pulse energy and a maximum pulse repetition frequency (PRF) of 10 Hz was used. The optoacoustic film transducer was set in 24.5 ℃ water and the expanded laser beam with about 30 mm diameter illuminated it with an approximately vertical angle. The produced acoustic waves were measured using a needle hydrophone (Φ = 0.2 mm, Precision Acoustics) with an 8 dB preamplifier and a digital oscilloscope (LeCroy LT354). The measured position was controlled using an *x*-*y*-*z* step motor.

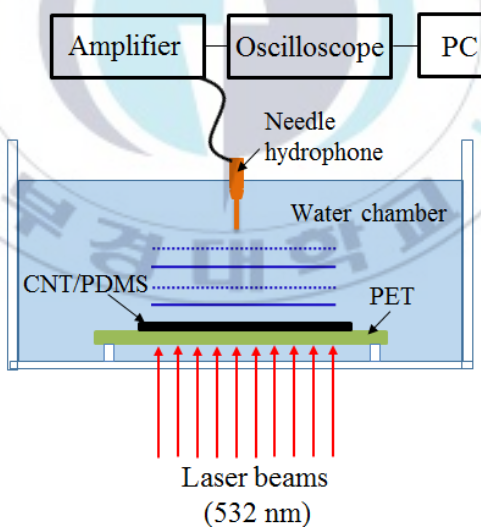

Fig. 6-1 Schematics of experimental setup.

6.1.2. Results

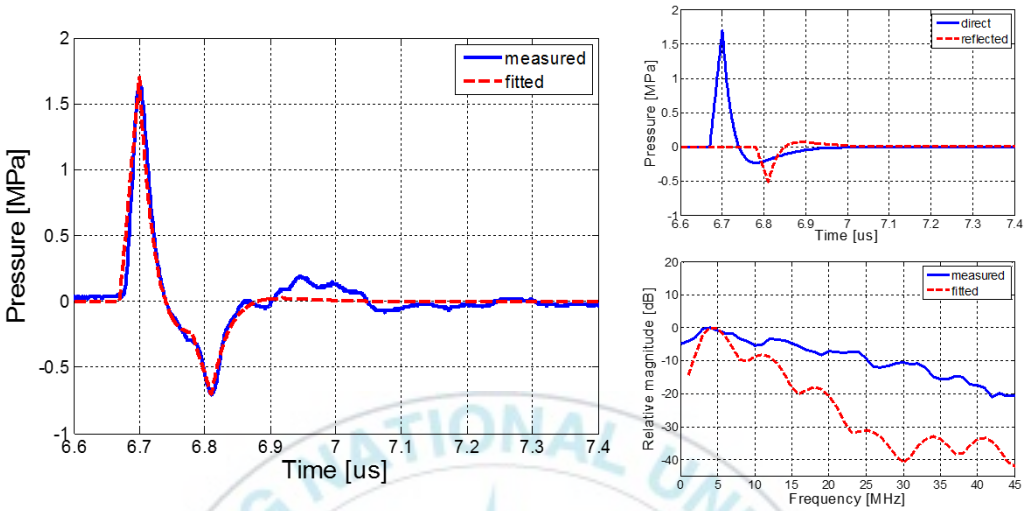

Fig. 6-2 Measured and fitted waveforms (a). Two shock wave components of the fitted waveform (b) and frequency spectra (c).

In Fig. 6-2(a), a typical waveform of the wave generated from the optoacoustic film transducer is shown with the waveform fitted by modification of the Friedlander equation [52, 62]. The equation gives the waveform after the peak pressure by explosion. In the modification, the pressure was assumed to increase linearly until it reached the peak pressure from the equilibrium. The waveform was measured at a position 10 mm from the transducer surface. When the laser energy was 150 mJ/pulse, the peak pressure was 1.7 MPa, and the -6 dB pulse width of the sharp positive (+) phase was about 27 ns. The pulse width varied with the laser energy within 20-30 ns. Because of the reflection from the bottom of the transducer, there was a peak in the negative (-) phase. On the other hand, the amplitude spectra in Fig. 6-2(c) show periodical patterns owing to the two shock waves of the direct propagation and bottom reflection as shown in Fig. 6-2(b). The measured and fitted waveforms were in good agreement. It reveals that the

film transducer produces a blast of wave-like shock waves owing to the thermoelastic effect.

Figures 6-3(a) and 6-3(b) show the variations of the waveforms and positive peak pressures with laser energy. The film transducer could tolerate laser energies higher than 300 mJ/pulse, and the positive peak pressure changed linearly with the laser energy and reached the maximum of 5.4 MPa at 330 mJ/pulse laser energy. When the laser energy was higher than 330 mJ/pulse, the acoustic pressure saturated and the CNT / PDMS film was damaged because of the high acoustic power.

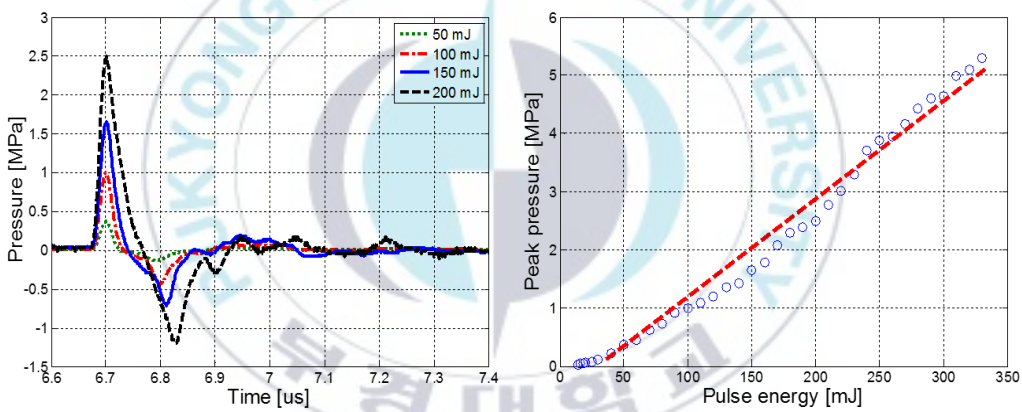

(a) (b)

Fig. 6-3 Variation of the waveform (a) and peak pressure (b) with laser energy for the film transducer.

6.2. Line-focused optoacoustic source

6.2.1. Structure of the line-focused optoacoustic source

Because the fabricated film transducer is thin and flexible, it is easy to fabricate different shapes of optoacoustic shock wave sources by attaching them onto a frame after tailoring. As an application of the film transducer, a cylindrical line-focused optoacoustic source with a radius of curvature r=14 mm and an aperture of 26 mm (L) x 10 mm (D) was fabricated as shown in Fig. 6-4(a). The tailored film transducer was attached onto a cylindrical frame with a rectangular aperture, which was formed using a 3D printer, as shown in Fig. 6-4(b).

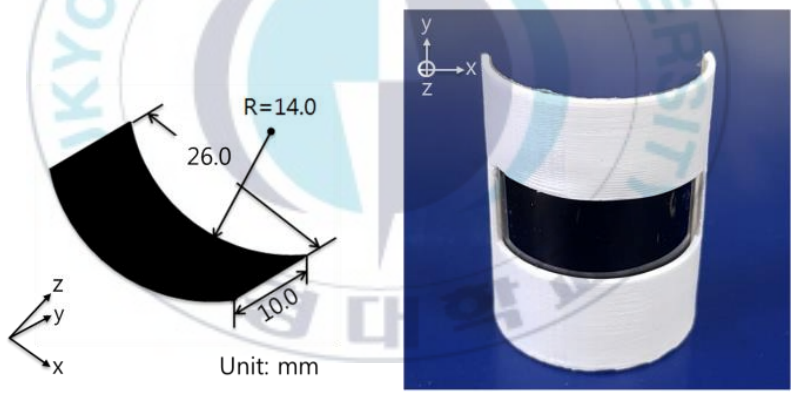

(a) (b)

Fig. 6-4 Structure (a) and photograph (b) of the CNT/PDMS line-focused optoacoustic source.

6.2.2. Characteristics of the ultrasound generated by the line-focused optoacoustic source

Figures 6-5(a) and 6-5(b) show the changes in the waveform and peak pressure with laser energy at the acoustic focus. Note that the line-focused optoacoustic source also produced a blast of a wave-like shock wave and the positive peak pressure changed linearly with laser energy. The positive peak pressure reached about 35 MPa at 330 mJ/pulse laser energy. Compared with Fig. 6-3(b), it is determined that the maximum positive peak pressure was amplified about 16 dB by the focusing effect of the source.

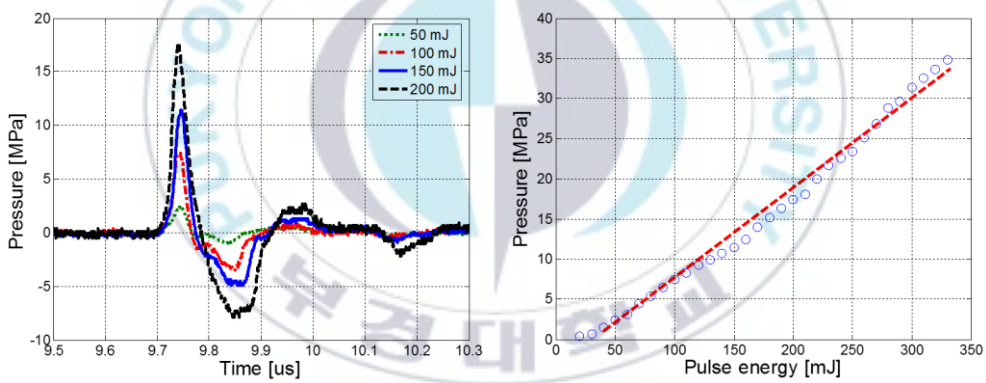

(a) (b)

Fig. 6-5 Variation of waveform (a) and peak pressure (b) with laser energy for the line-focused optoacoustic source.

Figure 6-6 shows the measured and simulated acoustic fields of the line-focused optoacoustic source. In the simulation using PZFlex software (Weidlinger Associates), it was assumed that the irradiated surface consisted of simple sources that generate the measured shock wave shown in Fig. 6-2(a). The simulated acoustic field [Fig. 6-6(b)] shows that the beam was markedly focused within 0.18 mm of the full width half maximum (FWHM) at the focal point. Owing to the limitations of the needle hydrophone size (0.2 mm) and the step size (0.1 mm) of the step motor, the measured field [Fig. 6-6(a)] was not as clear as the simulated field. However, it is shown that the focusing pattern of the measured field is similar to the simulated field.

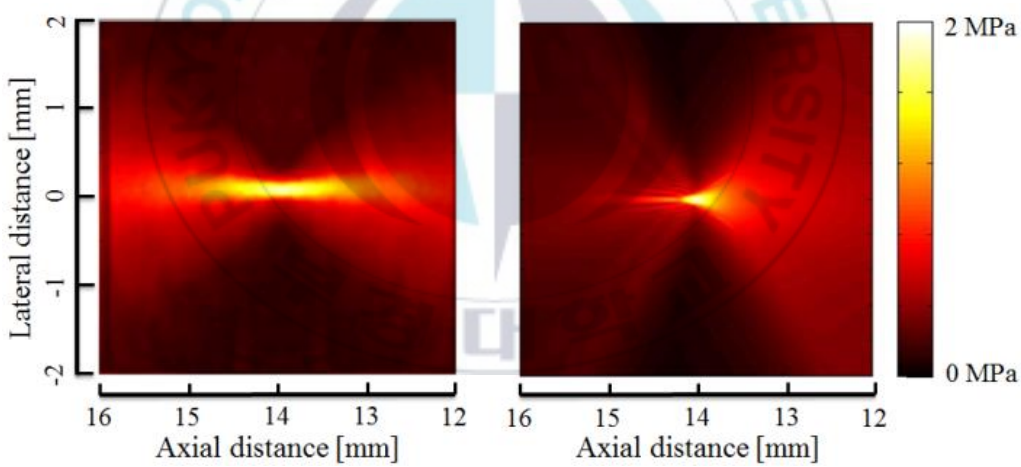

(a) (b)

Fig. 6-6 Measured (a) and simulated (b) acoustic fields generated by the line-focused optoacoustic source.

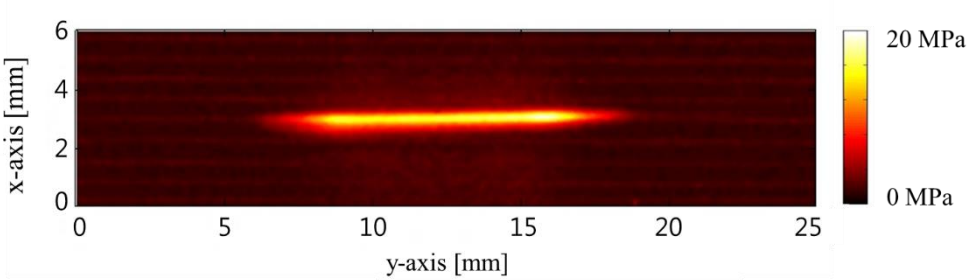

Fig. 6-7 Scanned image of the focal position of the line-focused optoacoustic source.

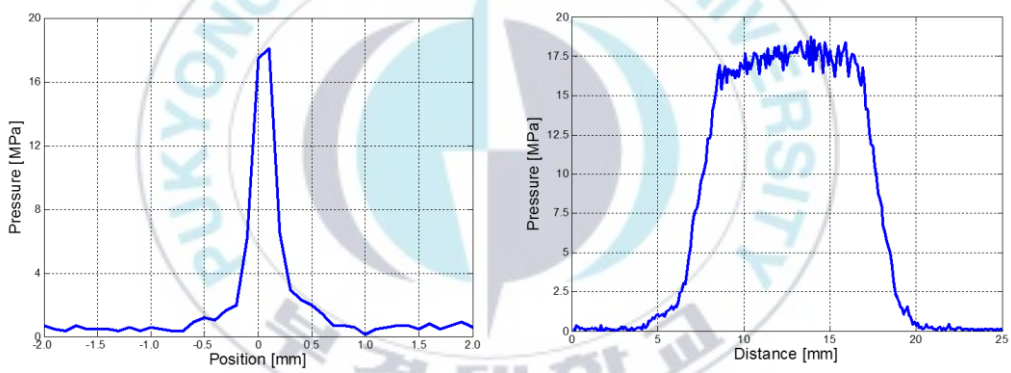

(a) (b)

Fig. 6-8 Pressure distribution across (a) the focal line and parallel (b) to the focal line of the line-focused optoacoustic source.

Figure 6-7 shows the measured acoustic field near the focal line of the line-focused optoacoustic source when the laser energy was 200 mJ/pulse. A line-type image with a high acoustic pressure is clearly shown in the figure. Figures 6-8(a) and 6-8(b) show the measured acoustic pressure distribution across (x) and parallel (y) to the focal line of the source. The acoustic pressure near the focal point was very sharply confined within 1.4 mm with 0.2 mm of FWHM and the peak pressure was about 17.5 MPa, as shown in Fig. 6-8(a). Owing to the inhomogeneity of laser intensity and the CNT/PDMS microstructure, there was some variation within $\pm$ 1.8 dB in the peak pressure, as shown in Fig. 6-8(b). The length of the peak pressure line was almost 10 mm, which corresponds to the width of the rectangular aperture on the cylindrical frame, and the acoustic pressure was confined within about 16 mm.

6.2.3. Applications of the line-focused optoacoustic source

(1) Microscale ultrasonic fragmentation of a chalk

The focusing effect of the acoustic pressure of the line-focused optoacoustic source was examined by applying the source to a chalk which was used as a kidney stone model. It demonstrated the microscale ultrasonic fragmentation of solid materials. It is shown that a line trace (black circle in Fig. 6-9) with length of about 10 mm was clearly engraved on the chalk surface. This result suggests that acoustic pressure for practical applications, such as ultrasonic fragmentation and biomedical therapy, may be obtained using the line-focused optoacoustic source with the film transducer.

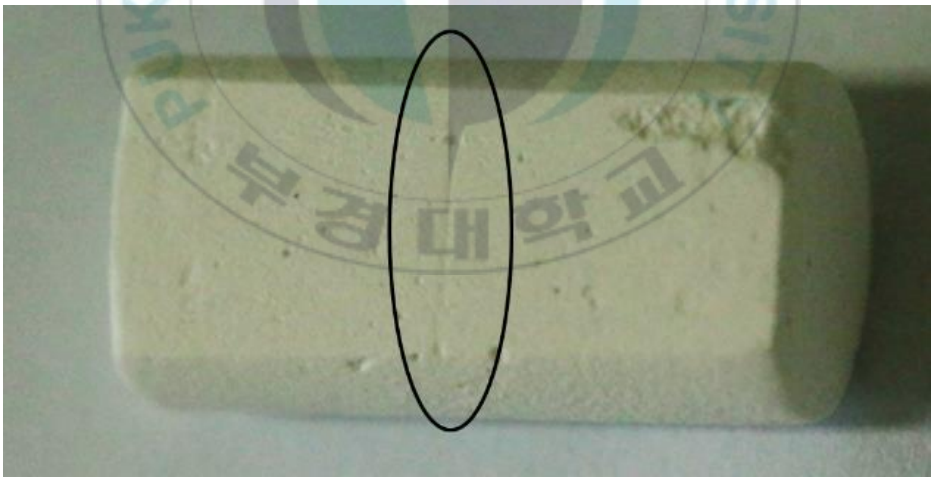

Fig. 6-9 Line (black circle) engraved on chalk owing to fragmentation effect of the line-focused optoacoustic source.

(2) Movement of microbubbles

Figure 6-10 show the experimental setup for observing the movement of microbubbles with the acoustic pressure by the line-focused source. The microbubbles were inserted in a small chamber and covered by with a cover glass. The microbubbles floated on the surface of the water in the chamber and located exactly at the focal position of the line-focused source. When the pulsed laser irradiated on the line-focused source, the generated ultrasonic pressure resulted in the movement of the microbubbles. The movement of the microbubbles were observed with an optical microscopy.

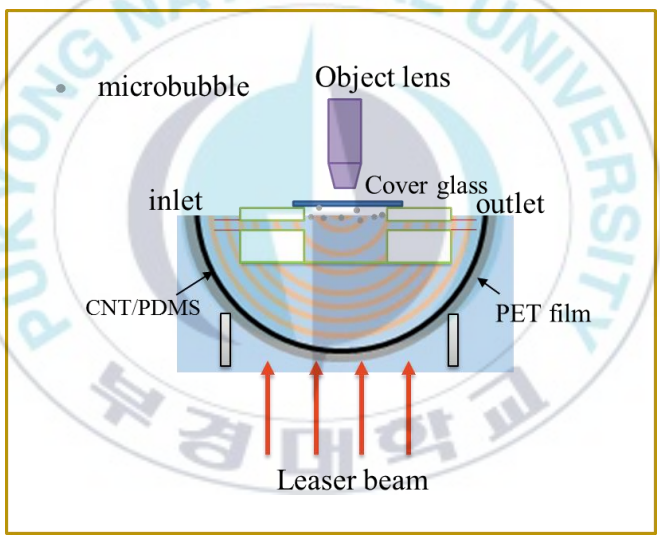

Fig. 6-10 Experimental setup for observing the movement of microbubbles with the acoustic pressure by the line-focused source.

Figure 6-11 shows the movement of the microbubbles under the acoustic pressure generated by the line-focused source. The laser energy was 300 mJ/pulse. After 20 pulsed laser irradiated on the line-focused source, it can be seen clearly that the microbubbles was separated in both sides of the focused line position. It indicates that

the acoustic pressure at the focused line position is very high.

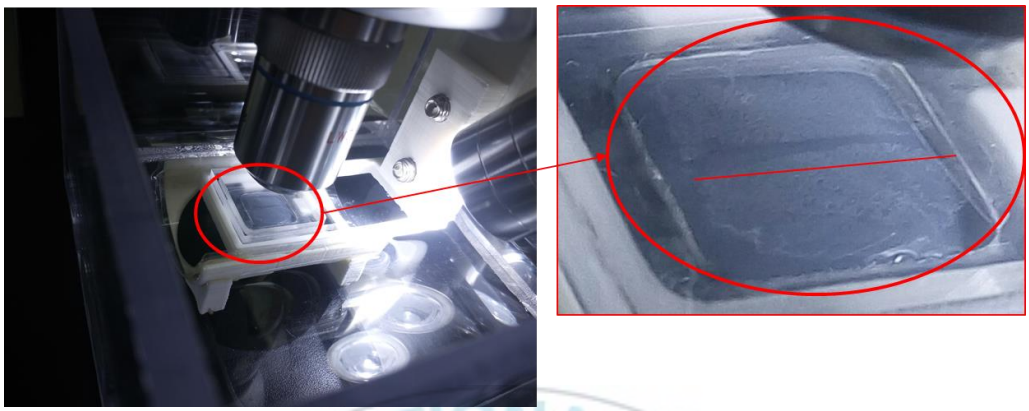

Fig. 6-11 Movement of the microbubbles under the acoustic pressure by the line-focused source. It can be seen clearly that the microbubbles was separated in both sides of the focused line position.

(3) Sonoporation effect on onion cells

Sonoporation is a transient increase in cell membrane permeability caused by cavitation phenomena during exposure to ultrasound. Sonoporation is of potential use as a method for gene delivery and drug delivery. Shock waves can result in sonoporation effect and create very high force that can perforate cell membranes and even permeabilize blood vessels.

Figure 6-12 shows the sonoporation effect on onion cells with the shock waves generated by the line-focused source. The onion cells floated on the water surface in the water chamber. The laser energy was 300 mJ/pulse. After 200 pulsed laser irradiated on the line-focused source, the membrane permeability of the onion cells was increased because of the pore formation in the membrane. The red circle in Fig. 6-13 shows that

more water went inside the onion cells.

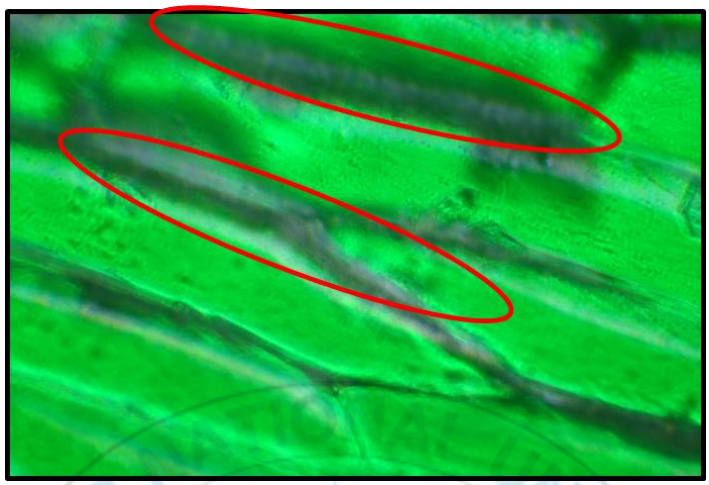

Fig. 6-12 Sonoporation effect on onion cells with the shock waves generated by the line-focused source.

6.3. Summary

The CNT/PDMS optoacoustic transducer with thin and flexible PET sheet can generated shock waves with very small pulse widths and high peak pressures. As an application, a line-focused optoacoustic source was fabricated using the film transducer. It generates a very high maximum pressure of about 35 MPa at its focal position and the measured field shows a strong focusing effect similar to the simulation result. From the line trace engraved on a chalk owing to the fragmentation effect, it is suggested that the acoustic pressure for microscale ultrasonic fragmentation and biomedical therapy may be obtained using a line-focused optoacoustic source with the film transducer.

Ch. 7. Conclusions

In this dissertation, the optoacoustic transducers have been well fabricated by coating CNT film and PDMS film on the surface of a PMMA substrate using vacuum filtration method and spin coating method, respectively.

It is demonstrated that the generated ultrasound waves from the CNT/PDMS optoacoustic transducers when irradiated pulsed laser have the blast wave-like shock waves which could be fitted well by Friedlander equation. The spin coated PDMS film has great influence on the peak pressure of the generated shock waves. However, the waveform doesn't have any significant dependence on the CNT film or the PDMS film thicknesses in the given range.

The propagation characteristics including sound speed and the attenuation coefficient of the blast waves in water were measured. From the comparison between the measurement and calculation of two-dimensional acoustic pressure fields, it is demonstrated that the generated ultrasound waves are planar shock waves.

The waveform of the generated ultrasound waves from the CNT/PDMS optoacoustic transducer when irradiated a pulsed laser was confirmed by using NDT transducers with narrow bandwidth considering the receiving impulse responses of the transducers. By comparing the calculated waveforms and the measured ones using commercial PVDF needle hydrophone and fiber optic hydrophone, it is confirmed that the generated ultrasound waves from the CNT/PDMS optoacoustic transducer when irradiated a pulsed laser are shock waves.

As an application, a line-focused optoacoustic source was fabricated using the CNT/PDMS optoacoustic transducer with flexible and thin PET substrate. It generates very high acoustic pressure about 35 MPa at its focal position and the measured field shows a strong focusing effect similar to the simulation result. From the line trace engraved on a chalk owing to the fragmentation effect, it is suggested that the acoustic pressure for microscale ultrasonic fragmentation and ESWT or ESWL may be obtained using the line-focused optoacoustic source.

References

[1] Allan Rosencwaig, *Photoacoustics and photoacoustic spectroscopy*. 1980: Wiley.

[2] Andrew C Tam, *Applications of photoacoustic sensing techniques.* Reviews of Modern Physics, 1986. **58**(2): 381.

[3] Alexander Graham Bell, *ART. XXXIV.--On the Production and Reproduction of Sound by Light.* American Journal of Science (1880-1910), 1880. **20**(118): 305.

[4] Alexander Graham Bell, *LXVIII. Upon the production of sound by radiant energy.* The London, Edinburgh, and Dublin Philosophical Magazine and Journal of Science, 1881. **11**(71): 510-528.

[5] Ernesto Marín, *Thermal wave physics: principles and applications to the characterization on liquids.* RECEN-Revista Ciências Exatas e Naturais, 2009. **6**(2): 145-169.

[6] Allan Rosencwaig and Allen Gersho, *Theory of the photoacoustic effect with solids.* Journal of Applied Physics, 1976. **47**(1): 64-69.

[7] Tsuyohiko Fujigaya, Shinsuke Haraguchi, Takahiro Fukumaru, et al., *Development of novel carbon nanotube/photopolymer nanocomposites with high conductivity and their application to nanoimprint photolithography.* Advanced Materials, 2008. **20**(11): 2151-2155.

[8] Ray H Baughman, Anvar A Zakhidov, and Walt A De Heer, *Carbon nanotubes--the route toward applications.* science, 2002. **297**(5582): 787-792.

[9] Hua Huang, CH Liu, Yang Wu, et al., *Aligned carbon nanotube composite films*

for thermal management. Advanced materials, 2005. **17**(13): 1652-1656.

[10] John David Anderson Jr, *Fundamentals of aerodynamics*. 2010: Tata McGraw-Hill Education.

[11] Gary S Settles, *High-speed imaging of shock waves, explosions and gunshots: New digital video technology, combined with some classic imaging techniques, reveals shock waves as never before.* American Scientist, 2006. **94**(1): 22-31.

[12] H. W. Baac, J. G. Ok, A. Maxwell, et al., *Carbon-nanotube optoacoustic lens for focused ultrasound generation and high-precision targeted therapy.* Sci Rep, 2012. **2**: 989.

[13] Richard J Colchester, Charles A Mosse, Davinder S Bhachu, et al., *Laser-generated ultrasound with optical fibres using functionalised carbon nanotube composite coatings.* Applied Physics Letters, 2014. **104**(17): 173502.

[14] Bao-Yu Hsieh, Jinwook Kim, Jiadeng Zhu, et al., *A laser ultrasound transducer using carbon nanofibers–polydimethylsiloxane composite thin film.* Applied Physics Letters, 2015. **106**(2): 021902.

[15] Akira Sakurai, *Blast wave theory*. 1964, WISCONSIN UNIV-MADISON MATHEMATICS RESEARCH CENTER.

[16] O Wess, F Ueberle, RN Duehrssen, et al., *Working group technical developments—consensus report.* High energy shock waves in medicine. Stuttgart: Thieme, 1997: 59-71.

[17] DM Wilbert, *A comparative review of extracorporeal shock wave generation.* BJU international, 2002. **90**(5): 507-511.

[18] Lawrence A Crum, *Cavitation microjets as a contributory mechanism for renal calculi disintegration in ESWL*. The Journal of urology, 1988. **140**(6): 1587-1590.

[19] M Delius, W Brendel, and G Heine, *A mechanism of gallstone destruction by extracorporeal shock waves.* Naturwissenschaften, 1988. **75**(4): 200-201.

[20] Yufeng Zhou, Franklin H Cocks, Glenn M Preminger, et al., *Innovations in shock wave lithotripsy technology: updates in experimental studies.* The Journal of urology, 2004. **172**(5): 1892-1898.

[21] Yuriy A Pishchalnikov, Oleg A Sapozhnikov, Michael R Bailey, et al., *Cavitation bubble cluster activity in the breakage of kidney stones by lithotripter shock waves.* Journal of endourology, 2003. **17**(7): 435-446.

[22] Jens J Rassweiler, Thomas Knoll, Kai-Uwe Köhrmann, et al., *Shock wave technology and application: an update.* European urology, 2011. **59**(5): 784-796.

[23] P Partheymüller, *Sonolith i-sys: the new standard in lithotripsy.* Therapeutic energy applications in urology II. Standards and recent developments. New York: Thieme, Stuttgart, 2010: 65-70.

[24] Yuri A Pishchalnikov, James A McAteer, R Jason VonDerHaar, et al., *Detection of significant variation in acoustic output of an electromagnetic lithotriptor.* The Journal of urology, 2006. **176**(5): 2294-2298.

[25] Sighard Schräbler, *Ein abtastendes Verfahren zur Darstellung und Analyse von Stoßwellen in Flüssigkeiten*. 1999: Shaker.

[26] Joachim Staudenraus and Wolfgang Eisenmenger, *Fibre-optic probe hydrophone for ultrasonic and shock-wave measurements in water.* Ultrasonics, 1993. **31**(4): 267-273.

[27] M Delius, F Ueberle, and S Gambihler, *Destruction of gallstones and model stones by extracorporeal shock waves.* Ultrasound in Medicine and Biology, 1994. **20**(3): 251-258.

[28] George K Chow and Stevan B Streem, *Extracorporeal lithotripsy: update on technology.* Urologic Clinics, 2000. **27**(2): 315-322.

[29] MR Bailey, VA Khokhlova, OA Sapozhnikov, et al., *Physical mechanisms of the therapeutic effect of ultrasound (a review).* Acoustical Physics, 2003. **49**(4): 369-388.

[30] JP Sferruzza, A Birer, and D Cathignol, *Generation of very high pressure pulses at the surface of a sandwiched piezoelectric material.* Ultrasonics, 2000. **38**(10): 965-968.

[31] OV Rudenko and OA Sapozhnikov. *Nonlinear Acoustics at the Beginning of the 21st Century*. in *Proc. 16th Int. Symposium on Nonlinear Acoustics*. 2002.

[32] Wolfgang Eisenmenger, *The mechanisms of stone fragmentation in ESWL.* Ultrasound in medicine and biology, 2001. **27**(5): 683-693.

[33] OV Rudenko and OA Sapozhnikov, *High-power acoustic beams: Self-action of discontinuous waves, focusing of pulses, and extracorporeallithotripsy(a review).* Moscow Univ. Phys. Bull, 1991. **46**: 5-18.

[34] Richard M White, *Generation of elastic waves by transient surface heating.* Journal of Applied Physics, 1963. **34**(12): 3559-3567.

[35] D. A. Hutchins, *Ultrasonic generation by pulsed lasers*, in *Physical Acoustics*. 1988, Elsevier. p. 21-123.

[36] Christopher B Scruby and Leslie E Drain, *Laser ultrasonics techniques and applications*. 1990: CRC Press.

[37] Sridhar Krishnaswamy, *Theory and applications of laser-ultrasonic techniques*, in *Ultrasonic nondestructive evaluation*. 2003, CRC press. p. 449-508.

[38] Yang Hou, Sheng-Wen Huang, Matthew O'Donnell, *Improvements in Optical Generation of High-Frequency Ultrasound.pdf*. ieee transactions on ultrasonics, ferroelectrics, and frequency control, 2007.

[39] G. C. Wetsel, *Photothermal generation of thermoelastic waves in composite media.* IEEE transactions on ultrasonics, ferroelectrics, and frequency control, 1986. **33**(5): 450-461.

[40] J. D. O'keefe and C. H. Skeen, *Laser‐induced stress‐wave and impulse augmentation.* Applied physics letters, 1972. **21**(10): 464-466.

[41] R. J. Von Gutfeld and H. F. Budd, *Laser‐generated MHz elastic waves from metallic‐liquid interfaces.* Applied Physics Letters, 1979. **34**(10): 617-619.

[42] F. Alan McDonald, *Practical quantitative theory of photoacoustic pulse generation.* Applied Physics Letters, 1989. **54**(16): 1504-1506.

[43] L. Fu and A. M. Yu, <*carbon nano materials based thin film- fabrication characteristics and application.pdf*>. Rev. Adv. Mater Sci., 2014. **36**: 40-61.

[44] B Safadi, R Andrews, and EA Grulke, *Multiwalled carbon nanotube polymer composites: synthesis and characterization of thin films.* Journal of applied polymer science, 2002. **84**(14): 2660-2669.

[45] Wen Ding, Vasileios Koutsos, Jin Hai Si, et al. *Study on the Morphology Properties*

of Carbon Nanotube/Polyaniline Composites Thin Film. in *Advanced Materials Research*. 2012. Trans Tech Publ.

[46] A Aguilar-Elguézabal, Wilber Antúnez, Gabriel Alonso, et al., *Study of carbon nanotubes synthesis by spray pyrolysis and model of growth.* Diamond and related materials, 2006. **15**(9): 1329-1335.

[47] Rong Xiang, Zhou Yang, Qiang Zhang, et al., *Growth deceleration of vertically aligned carbon nanotube arrays: Catalyst deactivation or feedstock diffusion controlled?* The Journal of Physical Chemistry C, 2008. **112**(13): 4892-4896.

[48] Yangxin Zhou, Liangbing Hu, and George Grüner, *A method of printing carbon nanotube thin films*. Applied physics letters, 2006. **88**(12): 123109.

[49] Kentaro Kobari, Yutaro Yamamoto, Masanori Sakuma, et al., *Fabrication of thin sensitive film of ball surface acoustic wave sensor by off-axis spin-coating method.* Japanese Journal of Applied Physics, 2009. **48**(7S): 07GG13.

[50] Chaehyun Lim, Dong-Hun Min, and Seung-Beck Lee, *Direct patterning of carbon nanotube network devices by selective vacuum filtration.* Applied Physics Letters, 2007. **91**(24): 243117.

[51] Hui Cao, Zhiyin Gan, Qiang Lv, et al., *Single-walled carbon nanotube network/poly composite thin film for flow sensor.* Microsystem Technologies, 2010. **16**(6): 955-959.

[52] Manmohan Dass Goel, Vasant A Matsagar, Anil K Gupta, et al., *An abridged review of blast wave parameters.* Defence Science Journal, 2012. **62**(5): 300-306.

[53] Kazuyoshi Takayama, *Application of underwater shock wave focusing to the development of extracorporeal shock wave lithotripsy.* Japanese journal of applied

physics, 1993. **32**(5S): 2192.

[54] N Smith, GN Sankin, WN Simmons, et al., *A comparison of light spot hydrophone and fiber optic probe hydrophone for lithotripter field characterization.* Review of Scientific Instruments, 2012. **83**(1): 014301.

[55] Hyoung Won Baac, Jong G Ok, Adam Maxwell, et al., *Carbon-nanotube optoacoustic lens for focused ultrasound generation and high-precision targeted therapy.* Scientific reports, 2012. **2**: 989.

[56] Lawrence E Kinsler, Austin R Frey, Alan B Coppens, et al., *Fundamentals of acoustics.* Fundamentals of Acoustics, 4th Edition, by Lawrence E. Kinsler, Austin R. Frey, Alan B. Coppens, James V. Sanders, pp. 560. ISBN 0-471-84789-5. Wiley-VCH, December 1999., 1999: 560.

[57] JMM Pinkerton, *The absorption of ultrasonic waves in liquids and its relation to molecular constitution.* Proceedings of the Physical Society. Section B, 1949. **62**(2): 129.

[58] Hyoung Won Baac, Jong G Ok, Hui Joon Park, et al., *Carbon nanotube composite optoacoustic transmitters for strong and high frequency ultrasound generation.* Applied physics letters, 2010. **97**(23): 234104.

[59] LH Tong, CW Lim, and YC Li, *Generation of high-intensity focused ultrasound by carbon nanotube opto-acoustic lens.* Journal of Applied Mechanics, 2014. **81**(8): 081014.

[60] C Moon, X Fan, K Ha, et al., *Generation of planar blast waves using carbon nanotubes-poly-dimethylsiloxane optoacoustic transducer.* AIP Advances, 2017. **7**(1): 015107.

[61] Xiaofeng Fan, Yonggeun Baek, Kanglyeol Ha, et al., *Propagation characteristics of shock waves from a plane carbon-nanotube-coated optoacoustic transducer in water.* Japanese Journal of Applied Physics, 2017. **56**(7S1): 07JB05.

[62] Frederick G Friedlander, *The diffraction of sound pulses I. Diffraction by a semi-infinite plane*. Proc. R. Soc. Lond. A, 1946. **186**(1006): 322-344.

Acknowledgements

Graduate school life has greatly improved me in the academic research and social interactions with other research groups during the past five years. Countless individuals contributed to the progress of my research ability and personal characteristics. I would like to give my greatest thanks to the persons who gave me help and influenced my thought over these years.

First, I would like to express my deepest gratitude to my advisor, Prof. Junghwan Oh, for his support on my master and doctoral study in Pukyong National University, and invaluable guidance towards my personality and experiments in the science world of the Biomedical. The word “change your mind” he said to me has become the motto of me. To me, Prof. Oh is a very kind and easygoing professor. I feel very fortunate for having Prof. Oh as my teacher and mentor.

Second, I would like to thank all my evaluation committee members, Prof. Kanglyeol Ha, Prof. Hyun Wook Kang, Prof. Moojoon Kim and Prof. Jungsoon Kim. Prof. Ha has given me the fundamentals knowledge of the acoustic field and invaluable and kind instruction in the completion of the experiments and thesis writing. I benefited a lot from the study with him. Prof. Hyun Wook Kang has been very friendly and always concerned with my progress and given me valuable suggestions on my experiments. Prof. Moojoon Kim has kindly supported me the equipment in his lab when I did experiment. Prof. Jungsoon Kim has been as friendly as an elder sister and her kindness has been very impressive.

Third, I would like to thank Prof. Yan-Lin Huang from Soochow University who helped me a lot before and after I came to Pukyong National University. Thanks to my Chinese friends Yonggang Cao, Peiqing Cai, Yanliang Liu, et al., for the happy time with them.

At last, I also have to say thanks to all my dear lab members and other colleagues, especially the friends Guansuk Kang, Ohbin Kwon, Seong Chan Kim, and Jooho Lee in Jeju National University, who are always willing to help me. I have learnt so much from them, and it is a wonderful time to study and discuss with them. It would have been lonely without them.

Most of all, I would also like to thank my parents and brothers for their unending love, sustained support and encouragement during these years when I left home.

Thanks to all of them.

Publications

1. **X. Fan**, K. Ha, M. Kim, G. Kang, M. J. Choi, and J. Oh ， Fabrication and application of a carbon nanotube/poly(dimethylsiloxane) coated optoacoustic film transducer, *Japanese Journal of Applied Physics*, 57, 07LB10 (2018).

2. **X. Fan**, Y. Baek, K. Ha, M. Kim, J. Kim, D. Kim, H. W. Kang, and J. Oh, Propagation characteristics of shock waves from a plane carbon-nanotube-coated optoacoustic transducer in water, *Japanese Journal of Applied Physics*, 56, 07JB05 (2017).

3. **X. Fan**, Y. Cao, K. Ha, M. Kim, H. W. Kang, and J. Oh, Fabrication of a PMN-PZT needle hydrophone for photoacoustic imaging, *The Journal of the Acoustical Society of Korea*, Vol.35, No.3 (2016).

4. C. Moon, **X. Fan**, K. Ha, and D. Kim, Generation of planar blast waves using carbon nanotubes-poly-dimethylsiloxane optoacoustic transducer, *AIP Advances* 7, 015107 (2017).

5. N.Q. Bui, K.K. Hlaing, V.P. Nguyen, T.H. Nguyen, Y.O. Oh, **X.F. Fan**, Y.W. Lee, S.Y. Nam, H.W. Kang, and J. Oh, Intravascular ultrasonic–photoacoustic (IVUP) endoscope with 2.2-mm diameter catheter for medical imaging, *Computerized Medical Imaging and Graphics* 45, 57-62, (2015).